



Synthesis and Evaluation of a Non-Peptide Small-Molecule Drug Conjugate Targeting Integrin $\alpha_v\beta_3$

Jannik Paulus and Norbert Sewald*

Organic and Bioorganic Chemistry, Department of Chemistry, Bielefeld University, Bielefeld, Germany

An integrin $\alpha_v\beta_3$ -targeting linear RGD mimetic containing a small-molecule drug conjugate (SMDC) was synthesized by combining the antimetabolic agent monomethyl auristatin E (MMAE), an enzymatically cleavable Val-Ala-PABC linker with a linear conjugable RGD mimetic. The structure proposal for the conjugable RGD mimetic was suggested upon the DAD mapping analysis of a previously synthesized small-molecule RGD mimetic array based on a tyrosine scaffold. Therefore, a diversifying strategy was developed as well as a novel method for the partial hydrogenation of pyrimidines in the presence of the hydrogenolytically cleavable Cbz group. The small-molecule RGD mimetics were evaluated in an ELISA-like assay, and the structural relationships were analyzed by DAD mapping revealing activity differences induced by structural changes as visualized in dependence on special structural motifs. This provided a lead structure for generation of an SMDC containing the antimetabolic drug MMAE. The resulting SMDC containing a linear RGD mimetic was tested in a cell adhesion and an *in vitro* cell viability assay in comparison to reference SMDCs containing cRGDfK or cRADfK as the homing device. The linear RGD SMDC and the cRGDfK SMDC inhibited adhesion of $\alpha_v\beta_3$ -positive WM115 cells to vitronectin with IC_{50} values in the low μM range, while no effect was observed for the $\alpha_v\beta_3$ -negative M21-L cell line. The cRADfK SMDC used as a negative control was about 30-fold less active in the cell adhesion assay than the cRGDfK SMDC. Conversely, both the linear RGD SMDC and the cRGDfK SMDC are about 55-fold less cytotoxic than MMAE against the $\alpha_v\beta_3$ -positive WM115 cell line with IC_{50} values in the nM range, while the cRADfK SMDC is 150-fold less cytotoxic than MMAE. Hence, integrin binding also influences the antiproliferative activity giving a targeting index of 2.8.

Keywords: integrins, RGD mimetics, linear conjugates, SAR study, SMDC, DAD mapping, $\alpha_v\beta_3$

1 INTRODUCTION

Targeted therapy devoid of side effects is a promising option in particular for cancer treatment. In this connection, antibody–drug conjugates (ADCs) (Gerber et al., 2009; Chari et al., 2014; Deneka et al., 2019; Hoppenz et al., 2020; Khongorzul et al., 2020) and small-molecule drug conjugates (SMDCs) (Srinivasarao et al., 2015; Deonarain et al., 2018; Hoppenz et al., 2020) were of great interest in the last decades. Such conjugates generally consist of a homing device (ADC: antibody; SMDC: small molecule/peptide), which addresses the desired receptor/cell and a payload (e.g., toxin) connected across a linker (stable or enzymatically/chemically cleavable) (Casi and Neri, 2015; Wei et al., 2018; Bargh et al., 2019; Hoppenz et al., 2020). Zoptarelin doxorubicin (Zoptrex™,

OPEN ACCESS

Edited by:

Rossella De Marco,
University of Udine, Italy

Reviewed by:

Andrea Sartori,
University of Parma, Italy
Carsten Hölte,
University Hospital Münster, Germany

*Correspondence:

Norbert Sewald
norbert.sewald@uni-bielefeld.de

Specialty section:

This article was submitted to
Medicinal and Pharmaceutical
Chemistry,
a section of the journal
Frontiers in Chemistry

Received: 04 February 2022

Accepted: 28 February 2022

Published: 11 April 2022

Citation:

Paulus J and Sewald N (2022)
Synthesis and Evaluation of a Non-
Peptide Small-Molecule Drug
Conjugate Targeting Integrin $\alpha_v\beta_3$.
Front. Chem. 10:869639.
doi: 10.3389/fchem.2022.869639

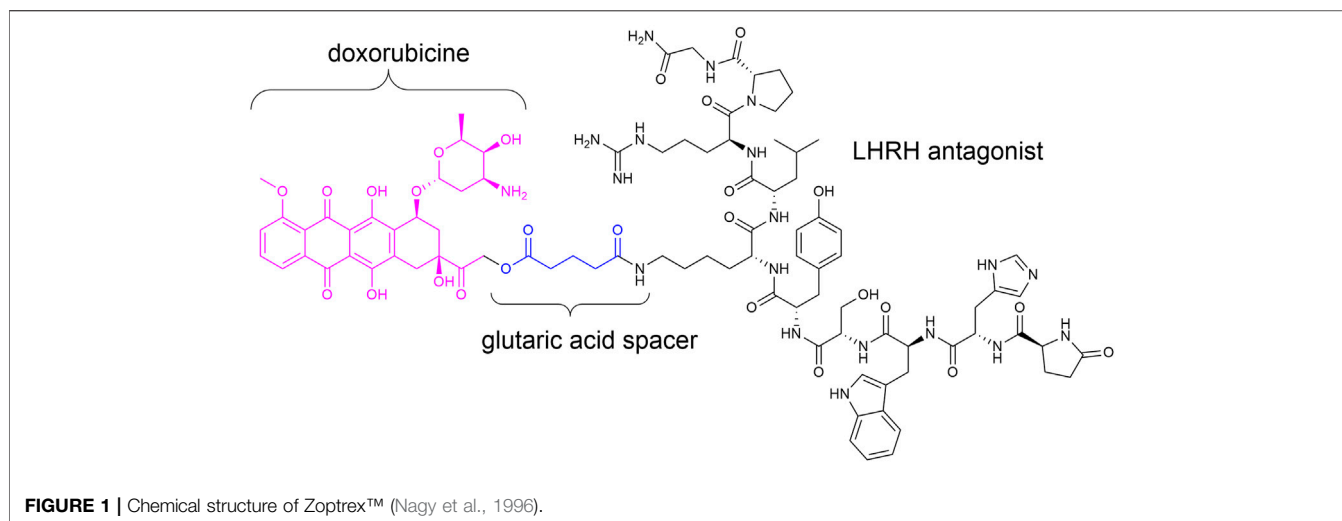


Figure 1 is an example for an SMDC that reached clinical phase III for endometrial cancer treatment. It is composed of doxorubicin connected across a glutaric acid spacer to a small peptide agonist of the luteinizing hormone-releasing hormone (LHRH) receptor (Rékási et al., 1993; Nagy et al., 1996; Engel et al., 2012; Hoppenz et al., 2020).

Integrins are important targets for drug conjugates. They consist of an α and a β unit, which are non-covalently associated. Currently, there are 24 unique integrin heterodimers known, formed from 18 α and eight β subunits (Humphries et al., 2006; Barczyk et al., 2010; Cooper and Giancotti, 2019). The integrins are located in the cell membrane and operate as a bidirectional connection between the extracellular matrix (ECM) and the cytoplasmic domain to transmit signals in both directions. The ectodomain acts as an aerial or an anchor to receive signals from other cells or the ECM and link between cells (cell adhesion protein) (Bachmann et al., 2019). Hence, it is not surprising that integrins are involved in many important processes like cell proliferation, migration, and angiogenesis (Eliceiri and Cheresch, 1999; Franceschi et al., 2015), which makes them attractive as a target to modulate cellular control mechanisms. Integrin $\alpha_v\beta_3$ is one of the most important representatives of the integrin family because of its significant impact in cellular processes (Giancotti and Ruoslahti, 1999; Hynes, 2002). It plays an important role in tumorigenesis because of its high expression level on tumor cells and its pro-angiogenic effect. This overexpression renders it a promising target in targeted cancer treatment. Therefore, integrin $\alpha_v\beta_3$ is the target in a multitude of SMDCs (Nahrwold et al., 2013; Dal Corso et al., 2016; Borbély et al., 2019a; Borbély et al., 2019b), dye conjugates (Jin et al., 2017; Kemker et al., 2021), or difunctionalized ligands, which consists of an α -Gal epitope and an integrin-addressing moiety for redirecting endogenous and immunogenic antibodies to cancer cells (Owen et al., 2007).

The tripeptide sequence Arg-Gly-Asp (RGD) present in many integrin ligands is recognized by eight of the 24 integrin heterodimers (Barczyk et al., 2010; Nieberler et al., 2017), and it is considered a universal recognition motif for cell-cell and

cell-ECM interactions. The selectivity for being recognized by a specific integrin is defined by the orientation, distance, and exposure of the essential residues and functional groups (Frank et al., 2010; Kapp et al., 2016; Kapp et al., 2017). Molecules which represent these properties and mimic the structural key elements are called RGD mimetics.

Since the early 1990s, Kessler and his group developed cyclic pentapeptides (Aumailley et al., 1991; Gurrath et al., 1992; Haubner et al., 1997) first with a high affinity for the integrin $\alpha_v\beta_3$ but a low selectivity against integrin $\alpha_5\beta_1$, which is also a RGD recognizing integrin (Schaffner et al., 2013). Later, *iso*DGR peptides (Frank et al., 2010; Bochen et al., 2013; Mas-Moruno et al., 2016a) and linear tyrosine-based RGD mimetics were investigated (Heckmann et al., 2007; Heckmann et al., 2009). The group of DeGrado designed and synthesized linear RGD mimetics with high affinity and high selectivity against integrin $\alpha_5\beta_1$ based on a diamine scaffold (Corbett et al., 1997; Rockwell et al., 1999). Most notably, in the last years, the cyclic cRGDfK peptide and its analogs [e.g., cyclo(*iso*DGR) and cyclo(DKP-RGD)] have been used as integrin $\alpha_v\beta_3$ -addressing homing devices in SMDCs (**Figure 2**) (Pina et al., 2017; Anselmi et al., 2020; Battistini et al., 2021; Lerchen et al., 2022).

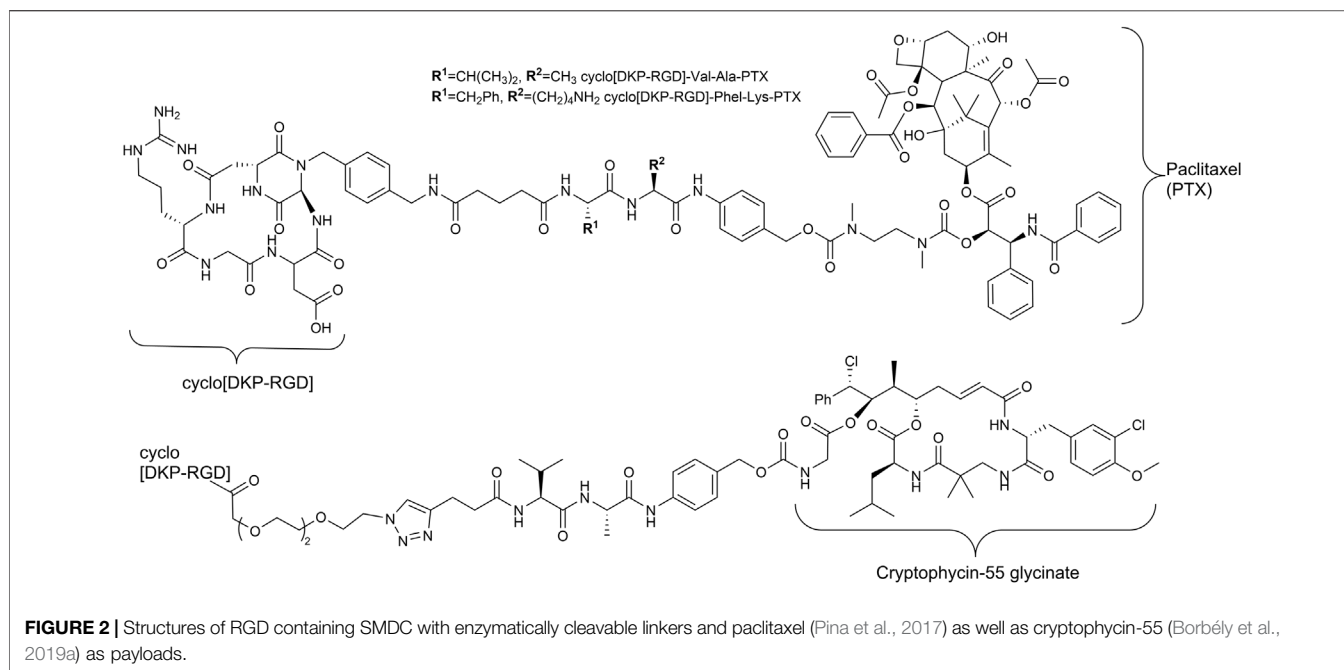
2 MATERIALS AND METHODS

2.1 General

Dichloromethane (DCM), petroleum ether, diethyl ether, and ethyl acetate were purchased at technical grade and distilled before usage. All other solvents were used as purchased (analytical grade). For further drying, DMF was stored over a molecular sieve (3 Å), and DCM was freshly distilled over CaH_2 and THF over sodium. Inert reactions took place under an argon atmosphere and in baked-out equipment.

2.2 NMR Spectroscopy

NMR spectra were recorded on a Bruker Avance 600 (600 MHz for ^1H , 564 MHz for ^{19}F , and 150 MHz for ^{13}C) and a Bruker



Avance III 500HD (500 MHz for ^1H , 126 MHz for ^{13}C , and 471 MHz for ^{19}F). The chemical shift δ is reported in ppm relative to the residual proton signal of the solvent: CDCl_3 7.26 ppm (^1H) and 77.2 ppm (^{13}C); $\text{DMSO}-d_6$ 2.50 ppm (^1H) and 39.52 ppm (^{13}C); CD_3OD 3.31 ppm (^1H) and δ 49.0 ppm (^{13}C). Two-dimensional methods (HMBC, HMQC, and COSY) were used to support and confirm the assignment.

2.3 LCMS and HRMS

LCMS analysis was performed by using an Agilent 6220 TOF-MS with a dual ESI source; 1200 HPLC system (Agilent) with an autosampler, degasser, binary pump, column oven, and diode array detector; and a Hypersil Gold C18 column (1.9 μm , 50 \times 2.1 mm). The gradient started with 100% A (water/ACN/formic acid, 94.9:5:0.1); during 11 min, the percentage of eluent B (ACN/water/formic acid, 94.9:5:0.1) increased from 0 to 98% B and returned to 0% B in 0.5 min. The total run time was 15 min at a flow rate of 0.3 ml/min and a column oven temperature of 40°C. After separation *via* the 1200 HPLC system, ESI mass spectra were recorded in an extended dynamic range mode equipped with a dual-ESI source, operating with a spray voltage of 2.5 kV. The same system was used for high-resolution mass spectrometry.

2.4 Purification by Column Chromatography/RP-HPLC

Normal column chromatography was performed with silica gel (particle size: 40–60 μm) from Merck. Automatic column chromatography (MPLC, medium-performance liquid chromatography) was carried out with a Büchi Reveleris X2 system and purchased columns. Polar compounds and final

products were purified *via* a preparative reverse-phase HPLC (RP-HPLC, Thermo Separation Products) consisting of a degasser, a pump (P4000), a Hypersil gold column (8 μm , 250 \times 21.2 mm cartridge; Thermo Fisher Scientific) and a UV detector (UV1000). The gradients were chosen depending on the compound with eluents A (water/ACN/TFA, 94.9:5:0.1) and B (ACN/water/TFA, 94.9:5:0.1).

2.5 Synthesis

2.5.1 General Procedure for Boc-Protection (GP-1)

Boc anhydride (1.2 eq) was dissolved in a mixture of water and dioxane and cooled to 0°C in an ice bath. Subsequently, the corresponding amino alcohol (1 eq.) was added, followed by addition of triethylamine (2 eq.). The reaction progress was monitored by TLC, and after full conversion, the reaction mixture was diluted with water and ethyl acetate. After phase separation, the water layer was extracted with ethyl acetate (3 \times), and the combined organic layers were washed with sat. NaCl (aq.) and dried over MgSO_4 . After evaporating the solvent, the desired *N*-Boc-protected amino alcohol was obtained as a highly viscous liquid and was used without further purification.

2.5.2 General Procedure for Mitsunobu-Reaction (GP-2)

The corresponding amino alcohol (1.1 eq.), Cbz-Tyr-OMe (1 eq.), and triphenylphosphine (1.2 eq.) were dissolved in dry THF in baked-out equipment under inert conditions. The solution was cooled to 0°C in an ice bath, and diisopropyl azodicarboxylate (DIAD, 1.2 eq.), dissolved in THF (30 ml), was added dropwise during 1.5 h. After removing the cooling bath, the reaction mixture was stirred overnight at room temperature. Subsequently, the solution was diluted with sat. NaHCO_3

(aq.), and the water layer was extracted with ethyl acetate (3 \times). The combined organic layers were dried over MgSO_4 , the solvent was removed under reduced pressure, and the crude product was purified by automatic column chromatography (MPLC, gradient of petroleum ether and ethyl acetate) to obtain the desired alkyl aryl ethers as a colorless foam.

2.5.3 General Procedure for Cbz-Cleavage (GP-3)

The Cbz-protected compound (1 eq.) was dissolved in MeOH, and Pd(OH)₂/C (10 % Pd, 0.1 eq.) was added to give a black suspension. Hydrogen was bubbled through the reaction mixture, and the reaction progress was monitored by LCMS. After full conversion, the suspension was filtered through a thin pad of celite. Afterward, the solvent was removed under reduced pressure, and the product was dried in vacuum to get the desired unprotected compound as a colorless solid.

2.5.4 General Procedure for N-Terminal Modification of RGD Mimetic Precursors With Acid Chlorides (GP-4a)

Triethylamine (3 eq.) was added to a solution of the corresponding unprotected compound (1 eq.) in 2 ml DMF/DCM (1:1, v:v), and after stirring for 5 min, benzoyl chloride (1.5 eq.) was added. The reaction progress was monitored *via* LCMS, and after full conversion, the solvent was removed. Afterward, the crude was dried in vacuum, and the resulting solid was dissolved in a small amount of water/ACN (1:1, v:v) and purified *via* preparative RP-HPLC.

2.5.5 General Procedure for N-Terminal Modification of RGD Mimetic Precursors With Carboxylic Acids (GP-4b)

HOBt solution (1.3 M in DMF, 1.3 eq.) was added to the corresponding 4- or 3-hydroxy benzoic acid (2.4 M in DMF, 1.2 eq.), followed by an EDC solution [0.5 M in DMF/DCM (1:1, v:v), 1.4 eq.] and DIPEA (2 eq.). The solution was stirred for 2 mins and was then added to the solution of the amino component **3a-c** (1 eq.) in DMF/DCM (1:1, v:v, 1 ml). The reaction mixture was stirred at room temperature, and the reaction progress was monitored by LCMS. After full consumption of the amine, the reaction was stopped by removing the solvent. Afterward, the crude was dried in vacuum, and the resulting solid was dissolved in a small amount of water/ACN (1:1, v:v) and purified *via* preparative RP-HPLC.

2.5.6 General Procedure for the Synthesis of Final RGD Mimetics—DHI Substituted (GP-5a)

HCl in dioxane (4 M, 100 μl , 13.3 eq.) was added to a solution of protected RGD mimetic precursors **5a-c**, **6a-c**, and **7a-c** (0.1 M in DCM, 300 μl , 1 eq.). After stirring for 1.5 h, the solvent was removed under reduced pressure, and a solution of 2-methylthio-2-imidazoline hydroiodide (0.18 M in MeOH/ NEt_3 1:1, v:v, 416 μl , 2.5 eq.) was added. The mixture was heated to 80°C in a sealed tube till consumption of the free amine (LC-MS), followed by solvent removal. The residue was then dissolved in a LiOH solution [0.285 M in MeOH/water (3:1, v:v), 526 μl , 5

eq.] and stirred at room temperature. Monitoring of the reaction progress was done *via* LCMS. After complete conversion, the crude mixture was concentrated and purified *via* preparative RP-HPLC.

2.5.7 General Procedure for the Synthesis of Final RGD Mimetics—Pyrimidine and THP Substituted (GP-5b-d)

It used **GP-5a** with 2-bromopyrimidine (0.36 M in MeOH/ NEt_3 1:1, v:v, 416 μl , 5 eq.) instead of 2-methylthio-2-imidazoline hydroiodide. After ester hydrolysis, the reaction batch was split into two equal amounts (1. **GP-5b** and 2. **GP-5c** or **GP-5d**), and the following procedure was applied:

GP-5b for pyr-substituted mimetics: Half of the reaction mixture was concentrated and purified *via* preparative RP-HPLC to obtain the pyrimidine-substituted final RGD mimetic.

GP-5c for THP in case of benzoyl-substituted mimetics: Half of the reaction mixture was combined with a suspension of Pd/C (10 mg ml^{-1} , 234 μl) and 100 μl acetic acid. Afterward, hydrogen was bubbled through the suspension till LC-MS showed full conversion. The reaction mixture was concentrated, centrifuged, and purified by preparative RP-HPLC to obtain the desired reduced RGD mimetic as TFA salt.

GP-5d for THP in case of Cbz-protected mimetics: Half of the reaction mixture was combined with Pd/C (10 % Pd, 0.1 eq.), 2-bromo-pyrimidine (10 eq.), HBr in AcOH (10 eq.), AcOH (200 eq.), and water (400 eq.) in MeOH to result in a 10 mM solution based on the half of the starting material. Hydrogen was bubbled through the suspension upon vigorous stirring till LC-MS showed full conversion. The reaction mixture was centrifuged, the solid residue was discarded, and the solution was diluted with water and freeze-dried. Afterward, the residue was purified by preparative RP-HPLC to obtain the desired reduced RGD mimetic as TFA salt.

2.5.8 Solid-Phase Peptide Synthesis (GP-6)

Resin loading: The Fmoc/^tBu strategy was chosen for the synthesis of linear peptides and peptide-based enzymatically cleavable linkers. Resin loading and subsequent coupling steps were performed in a syringe and on an automatic shaker. Barlos/2-chlorotrityl chloride resin (CTC-resin, 1.5 mmol/g) was swollen in DCM (10 ml/g resin) for 10–15 min at room temperature. Afterward, the solvent was removed, and a solution of the loading amino acid (1 eq. corresponding to resin) and DIPEA (10 eq.) in DCM (10 ml/g resin) was added. After incubation for 3 h at room temperature, MeOH (2 ml/g resin) was added, and the mixture was shaken for further 30 min. Then the resin was washed with DMF (5 \times) and DCM (3 \times) and dried in vacuum to determine the resin loading by a UV analysis of the piperidine–dibenzofulvene adduct formed upon cleavage of the Fmoc-protecting group with 20% piperidine in DMF.

Fmoc cleavage and coupling of amino acids: After resin loading, the resin was swollen in DMF for 10 min. Fmoc cleavage was performed twice with 20% piperidine in DMF (4 min in ultrasonic bath at 25°C, followed by 5 min on a shaker at r.t., 5 ml/g resin) and washing with DMF (5 \times 10 ml/g resin), DCM (2 \times 10 ml/g resin), and DMF (2 \times 10 ml/g resin). For the coupling

step, the corresponding amino acid (4 eq.), DIC (4 eq.), and oxyma (4 eq.) were dissolved in DMF (10 ml/g resin) and added to the reaction syringe containing the resin, followed by sonication for 4 min and further shaking for 5 min. Afterward, the resin was washed again with DMF (5 × 10 ml/g resin), DCM (2 × 10 ml/g resin), and DMF (2 × 10 ml/g resin). The coupling result was checked by the Kaiser test or analysis by LCMS after test cleavage. For the analysis, the resin was washed with DMF (5×) and DCM (3×) and dried in vacuum, and then approximately 10 beads were transferred into an Eppendorf tube and treated either with the reagents for the Kaiser test or with a mixture of TFA/TIS/MPW (95:2.5:2.5; 100 μ l) in case of the test cleavage. After incubation for 5 min, the test cleavage was diluted with 500 μ l of ACN/MPW (1:1) and analyzed by LCMS.

Cleavage from resin: Unless otherwise stated, the resin was swollen in DCM and treated 10 times with 1% TFA in DCM (5 ml). The resulting cleavage cocktail was passed into prepared *iso*-propanol, followed by evaporating the solvent and precipitation in Et₂O. After centrifugation, the resulting pellet was separated from the liquid residue and dried in vacuum.

2.5.9 Head-To-Tail Cyclization of Linear Peptides (GP-7)

The crude linear peptide was cyclized under pseudo-high-dilution conditions (Malesevic et al., 2004) without prior purification after cleavage. A solution of the peptide (1 eq.) in DMF and another solution with HATU (1.3 eq.) and HOAt (1.3 eq.) in DMF was prepared and added from two separate syringes to a solution of HATU (0.1 eq.), HOAt (0.1 eq.), and DIPEA (3 eq.) in DMF. The total DMF volume was chosen for a final peptide concentration of 10 mM. The peptide solution and the coupling reagent solution were added at a flow rate of 1.25 ml/h simultaneously to the stirred solution. After complete addition, stirring was continued overnight at room temperature. The solvent was evaporated in vacuum, followed by precipitation of the residue in Et₂O. The resulting pellet was dried and purified by normal-phase column chromatography (DCM/MeOH).

2.5.10 Allyl-Deprotection and Introduction of Linker Units to Cyclic RGD Mimetics (GP-8)

The resin was swollen in DMF (10 ml/g resin) and degassed by bubbling Ar through the suspension for 1 h, followed by addition of Pd(PPh₃)₄ (0.1 eq.) and 1,3-dimethylbarbituric acid (DMBA, 4 eq.). After 30-min shaking under inert conditions, the cleavage cocktail was removed, and the cleavage was repeated for further 30 min with fresh reagents. The resin was washed with DMF (5 × 10 ml/g resin), DCM (2 × 10 ml/g resin), and DMF (2 × 10 ml/g resin), followed by coupling of linker **23** (2 eq., **Supplementary Figure S9**) with oxyma (4 eq.) and DIC (4 eq.) corresponding to GP-6.

2.5.11 Synthesis of Final SMDCs (GP-9)

The corresponding conjugable RGD or RAD mimetic (2.2–2.3 eq.) was dissolved in a cleavage cocktail of TFA/MPW/TIS (1,400 μ l, 95:2.5:2.5) and stirred overnight at room

temperature. Afterward, the solvent was co-evaporated with toluene and dried in vacuum. The resulting residue was combined with linker-MMAE conjugate **13** (1 eq.) and sodium ascorbate (4.6–4.7 eq.) and dissolved in DMF (1,500 μ l) and MPW (200 μ l). This solution was degassed by several freeze–pump–thaw cycles and frozen in the end. Under inert conditions (Ar-atmosphere), CuSO₄·5H₂O (2.1–2.6 eq.) was added to the frozen degassed reaction mixture, followed by evacuation of the reaction vessel. The reaction mixture was allowed to warm up to room temperature and was stirred overnight, while the reaction progress was monitored by LCMS. When the consumption of linker-MMAE **13** was complete, the solution was frozen again, and Pd(PPh₃)₄ (0.4–0.5 eq.) and morpholine (4 eq.) were transferred into the reaction tube. The reaction was melted at room temperature and stirred for 2 h. After complete allyl deprotection, the reaction mixture was centrifuged and immediately purified by preparative RP-HPLC. The desired compound was obtained as a colorless solid.

2.5.12 Synthesis of Methyl 4-(2-(2-(2-azidoethoxy)ethoxy)ethoxy)benzoate (20)

Chloride **19** (**Supplementary Figure S8**, 0.753 g, 2.5 mol, 1 eq.) and NaN₃ (0.447 g, 6.9 mmol, 2.8 eq.) were dissolved in water (25 ml) and DMF (20 ml). The reaction mixture was stirred and heated overnight to 80°C and 1 day at room temperature. Afterward, the mixture was diluted with water and extracted with DCM (3×). The combined organic layers were washed with water (1×) and sat. NaCl (aq., 1×) and dried with MgSO₄, followed by removal of the solvent under reduced pressure. The product was dried in vacuum to obtain **20** (**Supplementary Figure S8**, 0.765 g, 2.5 mmol, 99%) as a light-yellow viscous liquid.

2.5.13 Synthesis of 5-Hexynoyl-Glu(AlI)-Val-Ala-PABA-PNPC (12)

The benzyl alcohol **25** (**Supplementary Figure S15**, 186.7 mg, 335.4 μ mol, 1 eq.) and bis(4-nitrophenyl) carbonate (256.7 mg, 843.9 μ mol, 2.5 eq.) were dissolved in dry DMF (6 ml), followed by addition of DIPEA (114.1 μ l, 670.9 μ mol, 2 eq.). The reaction mixture was stirred for 3 h, and the reaction progress was monitored using LCMS. After full conversion of the starting material, the reaction solution was added to a water/ACN/TFA solution (5:1 + 0.5 % TFA) and immediately frozen and freeze-dried. The resulting solid was purified by column chromatography [DCM→DCM/MeOH/TFA (95/4.9/0.1)] to give the activated linker **12** (194.4 mg, 269.3 μ mol, 80%) as a solid.

2.5.14 Synthesis of 5-Hexynoyl-Glu(AlI)-Val-Ala-PABA-MMAE (13)

A solution of activated linker **12** (59.9 mg, 83.0 μ mol, 1.1 eq.) and HOBt (1.3 mg, 8.42 μ mol, 0.1 eq.) in dry DMF (400 μ l) was added to a solution of MMAE (54.01 mg, 75.23 μ mol, 1 eq.) in dry DMF (400 μ l), followed by addition of pyridine (200 μ l). The reaction mixture was stirred at room temperature till full conversion of MMAE was observed by LCMS. Afterward, the reaction solution

TABLE 1 | Proteins and buffers applied in the ELISA-like assay.

Condition		Composition
$\alpha_v\beta_3$	(1)	1.0 $\mu\text{g/ml}$ human vitronectin
	(2)	2.0 $\mu\text{g/ml}$ human $\alpha_v\beta_3$ integrin
	(3)	2.0 $\mu\text{g/ml}$ mouse anti-human CD51/CD61
	(4)	1.0 $\mu\text{g/ml}$ anti-mouse IgG-POD goat
$\alpha_5\beta_1$	(1)	0.5 $\mu\text{g/ml}$ human fibronectin
	(2)	2.0 $\mu\text{g/ml}$ human $\alpha_5\beta_1$ integrin
	(3)	1.0 $\mu\text{g/ml}$ mouse anti-human CD51/CD61
	(4)	2.0 $\mu\text{g/ml}$ anti-mouse IgG-POD goat
Buffer	Carbonate	15 mM Na_2CO_3 , 35 mM NaHCO_3 , pH 9.6
	PBS-T	137 mM NaCl, 2.7 mM KCl, 10 mM Na_2HPO_4 , 2 mM KH_2PO_4 , 0.01% Tween 20
	TS-B	20 mM Tris-HCl, 150 mM NaCl, 1 mM CaCl_2 , 1 mM MgCl_2 , 1 mM MnCl_2 , pH 7.5, 1% BSA

was diluted with MPW and freeze-dried. The crude product was then purified by column chromatography [DCM->DCM/MeOH (90:10, v:v)] to give the linker-MMAE product **13** (94.6 mg, 72.7 μmol , 97%) as a colorless solid.

2.6 Biological Analysis and Methods

2.6.1 ELISA-Like Assay

An ELISA-like assay using the isolated extracellular domain of integrins $\alpha_v\beta_3$ and $\alpha_5\beta_1$ was performed in flat-bottom 96-well immuno plates (Brand) to determine the activities of the synthesized compounds. All wells were coated overnight with the native integrin ligand vitronectin or fibronectin (1) (**Table 1**) in a carbonate buffer (150 $\mu\text{l/well}$), followed by washing of each well with the PBS-T buffer ($3 \times 200 \mu\text{l/well}$) (**Table 1**) and blocking for 1 h with the TS-B buffer (150 $\mu\text{l/well}$) at RT. A dilution series was prepared using the internal standard (Cilengitide, 1:5 dilution) and the compounds (1:5 or 1:10 dilution) in the TS-B buffer. The protein-coated assay plate was washed with the PBS-T buffer ($3 \times 200 \mu\text{l/well}$), and 50 μl of the dilution series was transferred to the assay plate wells B–G. The TS-B buffer was filled into row A (100 $\mu\text{l/well}$) as the negative control and row H (50 $\mu\text{l/well}$) as the positive control. Afterward, the corresponding human integrin (2, 50 $\mu\text{l/well}$) (**Table 1**) in the TS-B buffer was added to row B–H and incubated for 1 h at RT. After washing the assay plate with the PBS-T buffer ($3 \times 200 \mu\text{l/well}$), the primary antibody (3, 100 $\mu\text{l/well}$) (**Table 1**) was transferred to each well and incubated for 1 h at RT. Then the plate was washed with the PBS-T buffer ($3 \times 200 \mu\text{l/well}$), treated with the secondary antibody (4, 100 $\mu\text{l/well}$) (**Table 1**), and incubated for 1 h at RT. The plate was washed with the PBS-T buffer ($3 \times 200 \mu\text{l/well}$), and SeramunBlau[®] fast2 (Seramun Diagnostics GmbH, 50 $\mu\text{l/well}$) was added to each well. Staining was stopped with 3 M aq. H_2SO_4 (50 $\mu\text{l/well}$) when the rows of the internal standard (cilengitide) showed a blue color gradient from well A to H ($\alpha_v\beta_3$: 40 s; $\alpha_5\beta_1$: 1.5 min). The absorbance was measured with a plate reader at 450 nm and corrected by subtraction of the absorbance at 620 nm. Afterward, the resulting values were plotted and analyzed using OriginPro[®] 2020b where the inflection point of a DoseResp fit describes the IC_{50} value. All compounds were tested in duplicates or triplicates for both integrins.

2.6.2 Flow Cytometry

WM115 and M21-L cells were seeded in 12-well plates or cell culture flasks and incubated at 37°C for one to 2 days. The cells were detached with Accutase solution (Pan Biotech), washed with the medium, and resuspended in the PBS buffer (137 mM NaCl, 2.7 mM KCl, 10 mM Na_2HPO_4 , 2 mM KH_2PO_4 , 300 μl). Then the primary antibody (1) (**Supplementary Table S2**) was added, followed by incubation for 15 min on ice. Subsequently, cells were centrifuged (10 min, 1800 rpm/350 g) and washed with PBS (800 μl , 10 min 1,800 rpm/350 g). After resuspension in PBS (300 μl), the secondary antibody (2) (**Supplementary Table S2**) was added, and the cells were incubated for 15 min on ice. Finally, the cells were centrifuged, washed, and resuspended as described and measured with an S3e Cell Sorter (BioRad) by excitation at 488 and 568 nm. For each sample, 30,000 events were measured. As controls, pure cells and cells treated only with the secondary antibody (2) (**Supplementary Table S2**) were measured. Results are shown in **Supplementary Figure S6**.

2.6.3 Cell Adhesion Assay

WM115 cells were cultivated and used in the MEM Eagle medium (Pan Biotech P04-08500 with 10% fetal bovine serum, 50 $\mu\text{g/ml}$ gentamycin, and 0.5 mM sodium pyruvate) and M21-L cells in the RPMI medium (Pan Biotech P04-16500 with 10% fetal bovine serum, 1% Pen-Strep). A flat-bottom MaxiSorp Nunc 96-well plate was coated with recombinant human vitronectin (100 $\mu\text{l/well}$, 1 $\mu\text{g/ml}$, Peprotech) in the PBS buffer (137 mM NaCl, 2.7 mM KCl, 10 mM Na_2HPO_4 , 2 mM KH_2PO_4 , pH 7.4) at 4°C and blocked at the following day by adding a solution of fatty acid free milk powder in PBS buffer (5 w/v %, 100 $\mu\text{l/well}$) at 4°C. The WM115 and M21-L cells were washed with the PBS buffer, detached with Accutase solution (5 ml, Pan Biotech P10-21100) at 37°C for 5 min, and then diluted with the medium (15 ml). After centrifugation (850 rpm, 6 min), the resulting cell pellet was resuspended with fluorescein diacetate in the medium (fluorescein diacetate 1.5 mg/ml, cell density 5×10^5 cells/ml) and incubated for 30 min at 37°C in the dark. The cells were washed twice with the medium and then resuspended in the medium (cell density 5×10^5 cells/ml). Afterward, a solution of CaCl_2 , MnCl_2 , and MgCl_2 (each 100 mM) in the PBS buffer (90 μl) was transferred to the cells and incubated for 30 min on ice in the

dark. In the meantime, a dilution series of the compounds in the medium (1:3 dilution) was prepared, and 240 μl were transferred to Eppendorf tubes. Pure medium was used as a positive control. Cell suspension (240 μl) was added to each tube of the dilution series and the control, followed by incubation at 37°C for 30 min in the dark. The assay plate was discharged and washed with 200 μl /well medium. Then the cell suspension with different compound concentrations was added to the assay plate (100 μl /well) and incubated for 60 min at 37°C in the dark. Afterward, the assay plate was washed with the medium (3 \times 100 μl /well), and finally, the medium (100 μl /well) was added and the fluorescence was measured with a TecanReader (Excitation: 480 nm; Emission: 520 nm). The determined values were plotted and analyzed using OriginPro[®] 2020b where the inflection point of a DoseResp fit described the IC_{50} value.

2.6.4 Cell Viability Assay

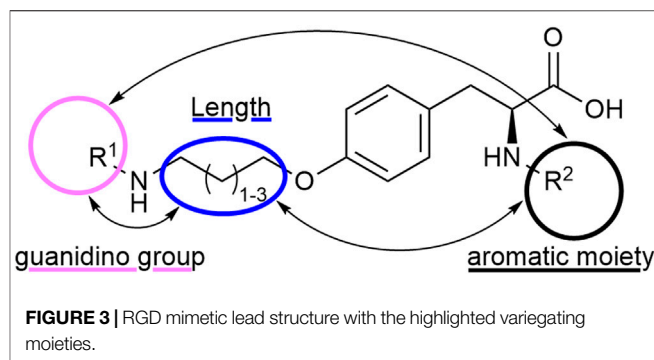
WM115 cells were cultivated in the MEM medium (with 10% fetal bovine serum, 50 $\mu\text{g}/\text{ml}$ gentamycin, and 0.5 mM sodium pyruvate) at 37°C and 5.3% CO_2 -humidified air in an incubator. The cells were seeded in a sterile flat-bottom cell culture 96-well plate (Sarstedt) in a density of 10,000 cells/well (100 μl /well) and incubated for 1 day as described. A serial dilution (1:3 dilution) of the compounds and the standard (cryptophycin-52) in the medium was prepared and transferred to the assay plate (100 μl /well), followed by incubation for 3 days as described. Afterward, a solution of resazurin (175 μM , 30 μl /well) was added, followed by incubation for 6 h. Subsequently, the fluorescence was measured with a TecanReader (Excitation: 530 nm; Emission: 588 nm) and plotted and analyzed using OriginPro[®] 2020b where the inflection point of a DoseResp fit described the IC_{50} value.

3 RESULTS AND DISCUSSION

Among the previously described small-molecule drug conjugates (SMDC) based on or inspired by peptides, there are only a few conjugates known for targeting the integrins (Dal Corso et al., 2016; Baiula et al., 2021; Lerchen et al., 2022; Slack et al., 2022), particularly $\alpha_v\beta_3$, with non-peptide homing devices. Such RGD mimetics provide additional possibilities of introducing structural elements and are metabolically more stable than peptides. Moreover, the generation of compound arrays is straightforward. We embarked on the development of SMDC using RGD mimetics as homing devices. For selection of promising structures, DAD (dual activity and difference) mapping (Medina-Franco et al., 2011) was used, a methodology to visualize activity/selectivity changes against two different receptors upon partial structural changes in an array of molecules.

3.1 Library Design and RGD Mimetic Synthesis

Tyrosine is a well-established scaffold for non-peptidic RGD mimetics. It lead to a variety of bioactive compounds and



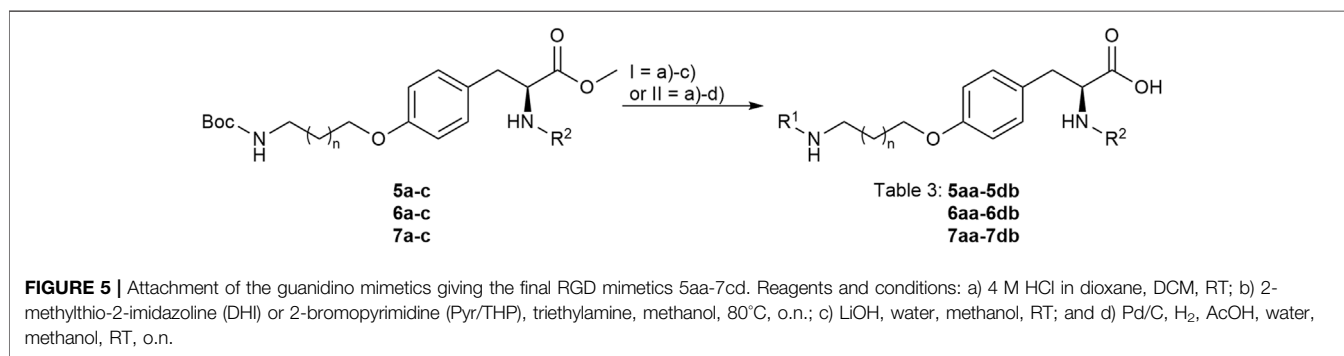
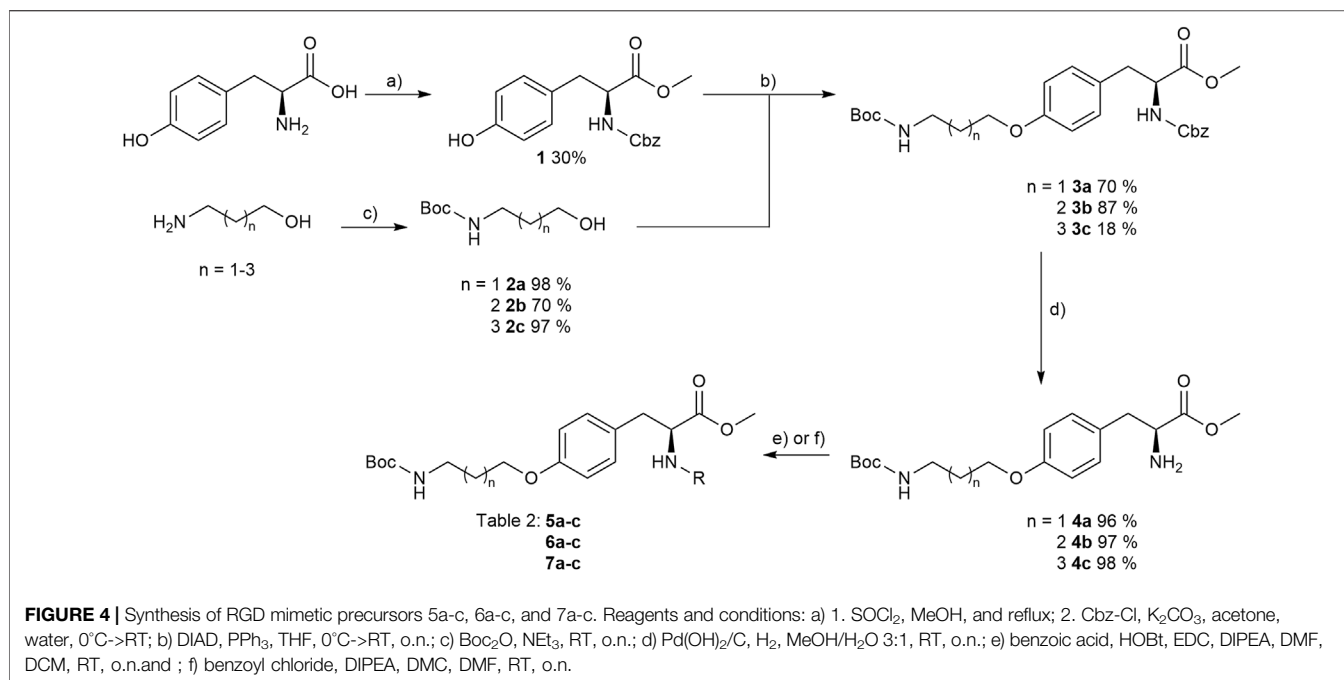
RGD mimetics like Tirofiban which is an antiplatelet medication by inhibition of the protein–protein interactions between fibrinogen and integrin $\alpha_{\text{IIb}}\beta_3$ (Egbertson et al., 1994; Curley et al., 1999) or selective inhibitors for integrin $\alpha_v\beta_3/\alpha_5\beta_1$ (Heckmann et al., 2007; Heckmann et al., 2008; Heckmann et al., 2009). In contrast to previous approaches, where one or two structural moieties were varied, an approach with variation of three parameters was chosen. Therefore, all possible permutations, depending on the chosen residues, were synthesized. The advantage of this strategy is that every structural change can be observed in all possible structural environments which may lead to a more meaningful SAR study (Figure 3).

A diversifying strategy was employed to generate an array of RGD mimetics using a minimum number of reaction steps by varying the distance (connector unit) between the guanidino-like group (R^1) and the carboxylic acid, introducing different guanidino analogs (R^1) and exchanging the *N*-terminal aromatic moiety (R^2 , Figure 3).

The reaction sequence started with the formation of Cbz-*L*-tyrosine methyl ester **1**, followed by the first diversification step etherifying the tyrosine phenol by MITSUNOBU reaction with three different Boc-protected amino alcohols **2a–c** as connector units. The Cbz-protected amines of the RGD mimetic precursors **3a–c** were deprotected by hydrogenolysis in the presence of $\text{Pd}(\text{OH})_2/\text{C}$. In the next step three different benzoyl substituents were introduced using the corresponding acid chloride or HOBt/EDC mediated amide formation (Figure 4 and Table 2).

The final reaction sequence comprises three to four steps without purification of intermediate products. After acidolysis of the Boc group the guanidino mimetics were attached. The 2-imidazoline-2-yl moiety (DHI) was introduced using 2-methylthio-2-imidazoline, while the pyrimidin-2-yl residue (Pyr) was attached using 2-bromopyrimidine. The methyl ester was saponified with an excess of LiOH in water/methanol (3:1, *v:v*). The tetrahydropyrimidin-2-yl derivative (THP) as guanidino analog was obtained by catalytic hydrogenation of the pyrimidin-2-yl derivatives in the presence of AcOH to avoid the complexation of Pd by the guanidine-like groups (Figure 5 and Table 3).

In order to obtain the THP derivatives **5dc**, **6dc**, and **7dc** containing a Cbz group, a modified procedure for the pyrimidine reduction without cleaving Cbz was required (Figure 6).



Interestingly, under reduction conditions II (Figure 5 and Table 3), the expected Cbz cleavage was slow and even in one case the THP derivative could be isolated. Closer investigation of the reaction and improvement of conditions II (Figure 5 and Table 3) resulted in a method for the selective reduction of the pyrimidine ring in the presence of the Cbz group. Noteworthy, 2-bromopyrimidine poisons the Pd catalyst and leads to a selective reduction of the pyrimidine moiety without cleaving the

reduction labile Cbz group, while addition of HBr or HCl suppresses side reactions (Figure 6).

3.2 Competitive Integrin Binding Assay

The affinities (Table 4) of the RGD mimetics (Table 3) toward the integrins $\alpha_V\beta_3$ and $\alpha_5\beta_1$ were determined in a competitive enzyme-linked immunosorbent assay (ELISA) using recombinant human integrins with the native ligands

TABLE 2 | Yields and methods for the final reaction step of Figure 4 where e) applies to I and f) to II.

Length	Yield [%]			Yield [%]			Yield [%]		
n = 1	5a	II	39	5b	II	51	5c	I	26
n = 2	6a	II	38	6b	II	38	6c	I	35
n = 3	7a	II	26	7b	II	24	7c	I	33

TABLE 3 | Yields for the reaction sequence in **Figure 5** and **Figure 6**.

R^2									
R^1	Length	Yield [%]	Yield [%]	Yield [%]	Yield [%]	Yield [%]	Yield [%]	Yield [%]	Yield [%]
	$n = 1$	5aa 60	5ba 62	5ca 43	5da 68				
	$n = 2$	6aa 21	6ba 49	6ca 45	6da 61				
	$n = 3$	7aa 86	7ba 73	7ca 55	7da 62				
	$n = 1$	5ab 28	5bb 30	5cb 42	5db 90				
	$n = 2$	6ab 33	6bb 78	6cb 39	6db 70				
	$n = 3$	7ab 37	7bb 41	7cb 10	7db 38				
	$n = 1$	5ac 9	5bc 18	5cc 61	5dc 27				
	$n = 2$	6ac 14	6bc 79	6cc 47	6dc 28				
	$n = 3$	7ac 15	7bc 10	7cc 43	7dc 12				

vitronectin and fibronectin as described in the literature (Mas-Moruno et al., 2016b).

Most of the RGD mimetics investigated display higher affinity to integrin $\alpha_V\beta_3$, with only a few compounds with a linker length of $n = 1$ or 2, a DHI/THP guanidino mimetic and a benzoyl derivative at the Tyr nitrogen preferring integrin $\alpha_5\beta_1$. Based on the chosen guanidino analogs it was expected that all mimetics should favor the α_V -subunit by preventing hydrogen bonds to a glutamic acid side chain (Q221) of the α_5 -subunit (Kapp et al., 2016). Furthermore, the Pyr derivatives generally display less affinity toward both integrins. Several RGD mimetics have high affinity to integrin $\alpha_V\beta_3$ with good selectivity over integrin $\alpha_5\beta_1$ whereupon in direct comparison (see **Supplementary Figure S1**) the longer ($n = 2-3$), Cbz substituted and DHI modified compounds as well as some of the hydroxybenzoyl derivatives showing an outstanding selectivity as well as activity (**6da**, **6dc**, **7ba**, **7da**, and **7dc** in **Table 4**).

3.3 DAD Mapping Analysis

The information gain of direct comparison between molecules/activities among each other is limited and the possible predictions are imprecisely for planning further modifications like the right composition of a conjugable RGD mimetic. Homology modeling

as a theoretical approach is a method to explain activity changes by docking ligands into a calculated 3D model of a structural unknown protein (Marinelli et al., 2005; Heckmann et al., 2007; Heckmann et al., 2008).

Another approach to overcome this obstacle is to visualize the impact of structural changes by creating DAD (dual activity and difference) maps. These maps were developed by Jose L. Medina-Franco (Pérez-Villanueva et al., 2011; Medina-Franco, 2012) to point out what consequence a structural change is effecting in dependence of two or more receptors/targets (Medina-Franco et al., 2013). Therefore, the affinity/activity difference, in a logarithmic scale, of two compounds for one specific target is presented on the X-axis and for the second target on the Y-axis. The amount of deflection from the center describes the magnitude of the affinity and selectivity change that is evoked through this variation as well as the direction of deflection shows the nature of the effect (**Figure 7**).

The IC_{50} affinity values of the RGD mimetics toward the integrins $\alpha_V\beta_3$ and $\alpha_5\beta_1$ (**Table 4**) were used to create DAD maps for each parameter (length, guanidino mimetic, and aromatic moiety). One parameter was fixed, and a structural change in the second parameter is marked in color (**Figure 8**). The changes in the third parameter were disregarded. The common logarithm of

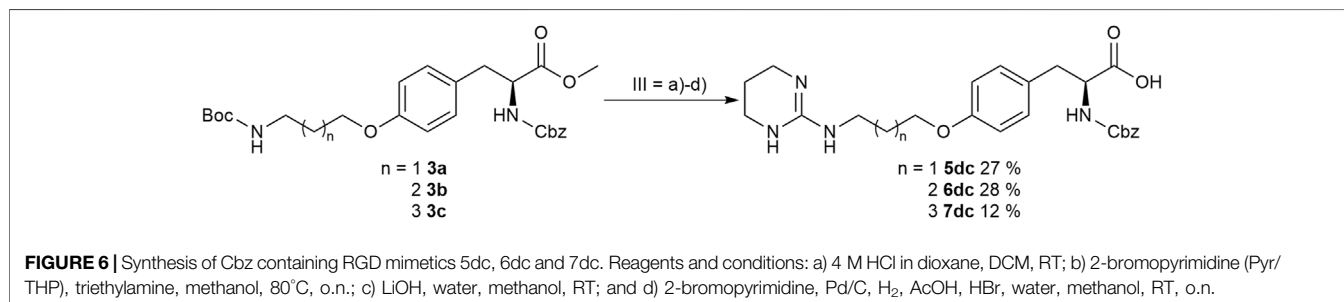


TABLE 4 | Results of the ELISA-like assay with the isolated extracellular domains of integrin $\alpha_V\beta_3$ and $\alpha_5\beta_1$. Cilengitide (IC_{50} $\alpha_V\beta_3$: 0.54 nM; $\alpha_5\beta_1$: 15.4 nM) was used as reference for all assay plates.

ID	n =	R ¹	R ²	Integrin $\alpha_V\beta_3$	Integrin $\alpha_5\beta_1$
				IC ₅₀ [nM]	IC ₅₀ [nM]
5aa	1	DHI	Benzoic acid	38.5 ± 24.3	25.2 ± 7.35
5ba	1	DHI	4-OH benzoic acid	38.8 ± 19.2	43.4 ± 24.4
5ca	1	DHI	3-OH benzoic acid	9.29 ± 5.77	30.5 ± 20.7
5da	1	DHI	Cbz	1.32 ± 0.11	162 ± 36.0
5ab	1	Pyr	Benzoic acid	1,311 ± 4.51	>10,000
5bb	1	Pyr	4-OH benzoic acid	6,530 ± 454	>10,000
5cb	1	Pyr	3-OH benzoic acid	7,701 ± 416	>10,000
5db	1	Pyr	Cbz	237 ± 69.7	>10,000
5ac	1	THP	Benzoic acid	18.1 ± 3.68	17.4 ± 3.34
5bc	1	THP	4-OH benzoic acid	70.4 ± 0.57	18.5 ± 3.65
5cc	1	THP	3-OH benzoic acid	452 ± 120	32.8 ± 11.2
5dc	1	THP	Cbz	4.68 ± 4.47	71.6 ± 16.1
6aa	2	DHI	Benzoic acid	25.8 ± 6.77	175 ± 73.7
6ba	2	DHI	4-OH benzoic acid	1896 ± 175	35.2 ± 18.4
6ca	2	DHI	3-OH benzoic acid	1.01 ± 0.56	19.9 ± 8.7
6da	2	DHI	Cbz	1.20 ± 0.11	901 ± 223
6ab	2	Pyr	Benzoic acid	6,166 ± 1779	>10,000
6bb	2	Pyr	4-OH benzoic acid	5,289 ± 1,106	>10,000
6cb	2	Pyr	3-OH benzoic acid	1850 ± 241	>10,000
6db	2	Pyr	Cbz	8,286 ± 4,393	>10,000
6ac	2	THP	Benzoic acid	32.8 ± 17.6	17.5 ± 6.76
6bc	2	THP	4-OH benzoic acid	38.7 ± 15.5	511 ± 183
6cc	2	THP	3-OH benzoic acid	90.4 ± 31.3	107 ± 32.0
6dc	2	THP	Cbz	0.57 ± 0.03	745 ± 117
7aa	3	DHI	Benzoic acid	38.5 ± 9.02	1,687 ± 748
7ba	3	DHI	4-OH benzoic acid	2.01 ± 0.40	1,652 ± 441
7ca	3	DHI	3-OH benzoic acid	98.1 ± 74.8	6,077 ± 3,070
7da	3	DHI	Cbz	3.76 ± 1.98	7,746 ± 551
7ab	3	Pyr	Benzoic acid	8,766 ± 759	>10,000
7bb	3	Pyr	4-OH benzoic acid	8,835 ± 1,268	>10,000
7cb	3	Pyr	3-OH benzoic acid	2,887 ± 1,519	>10,000
7db	3	Pyr	Cbz	2,625 ± 1,114	8,359 ± 2,598
7ac	3	THP	Benzoic acid	58.8 ± 14.4	2,773 ± 899
7bc	3	THP	4-OH benzoic acid	36.4 ± 14.3	103 ± 54.4
7cc	3	THP	3-OH benzoic acid	42.9 ± 9.47	210 ± 44.8
7dc	3	THP	Cbz	2.93 ± 0.12	>10,000

its affinity (IC_{50}) toward an integrin ($\alpha_X\beta_Y$) was calculated for each compound **Mx** ($pIC_{50, Mx, integrin \alpha_X\beta_Y}$). Then each value was pairwise compared to all other values using Eq. 1, as follows:

$$\Delta pIC_{50, M1 \rightarrow M2, integrin \alpha_X\beta_Y} = pIC_{50, M1, integrin \alpha_X\beta_Y} - pIC_{50, M2, integrin \alpha_X\beta_Y} \quad (1)$$

where $M1 \rightarrow M2$ indicates the structural change from molecule $M1$ to another molecule $M2$. The resulting $\Delta pIC_{50, M1 \rightarrow M2, integrin \alpha_X\beta_Y}$ may have positive or negative values depending on the affinity gain or loss upon the structural change. A value of $\Delta pIC_{50, M1 \rightarrow M2, integrin \alpha_X\beta_Y} = 0$ represents no change in affinity based on the structural change for the specific integrin (Medina-Franco et al., 2013).

The DAD maps in Figure 8 present the affinity change for integrin $\alpha_V\beta_3$ on the X-axis and for integrin $\alpha_5\beta_1$ on the Y-axis depending on different selected structural changes. Panel A (Figure 8) confirms the assumption that a change to a pyrimidinyl group as R^1 in each structural environment leads to generally lower affinities and selectivity.

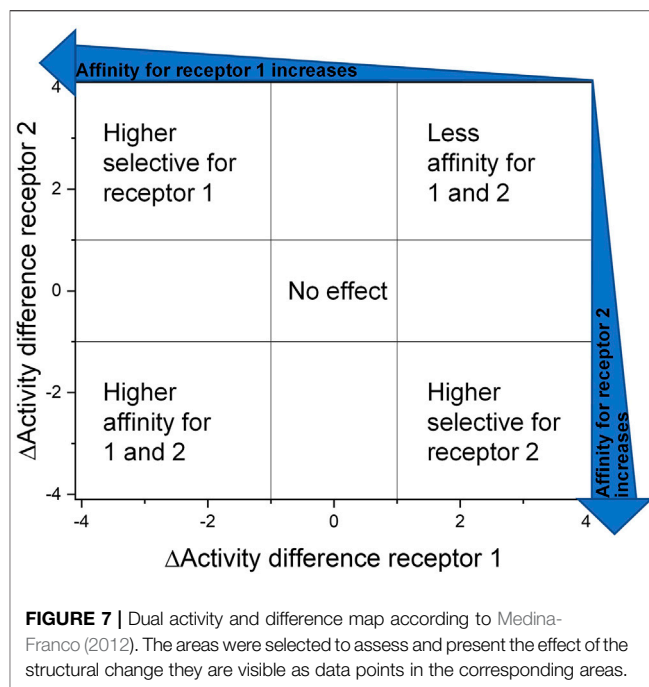
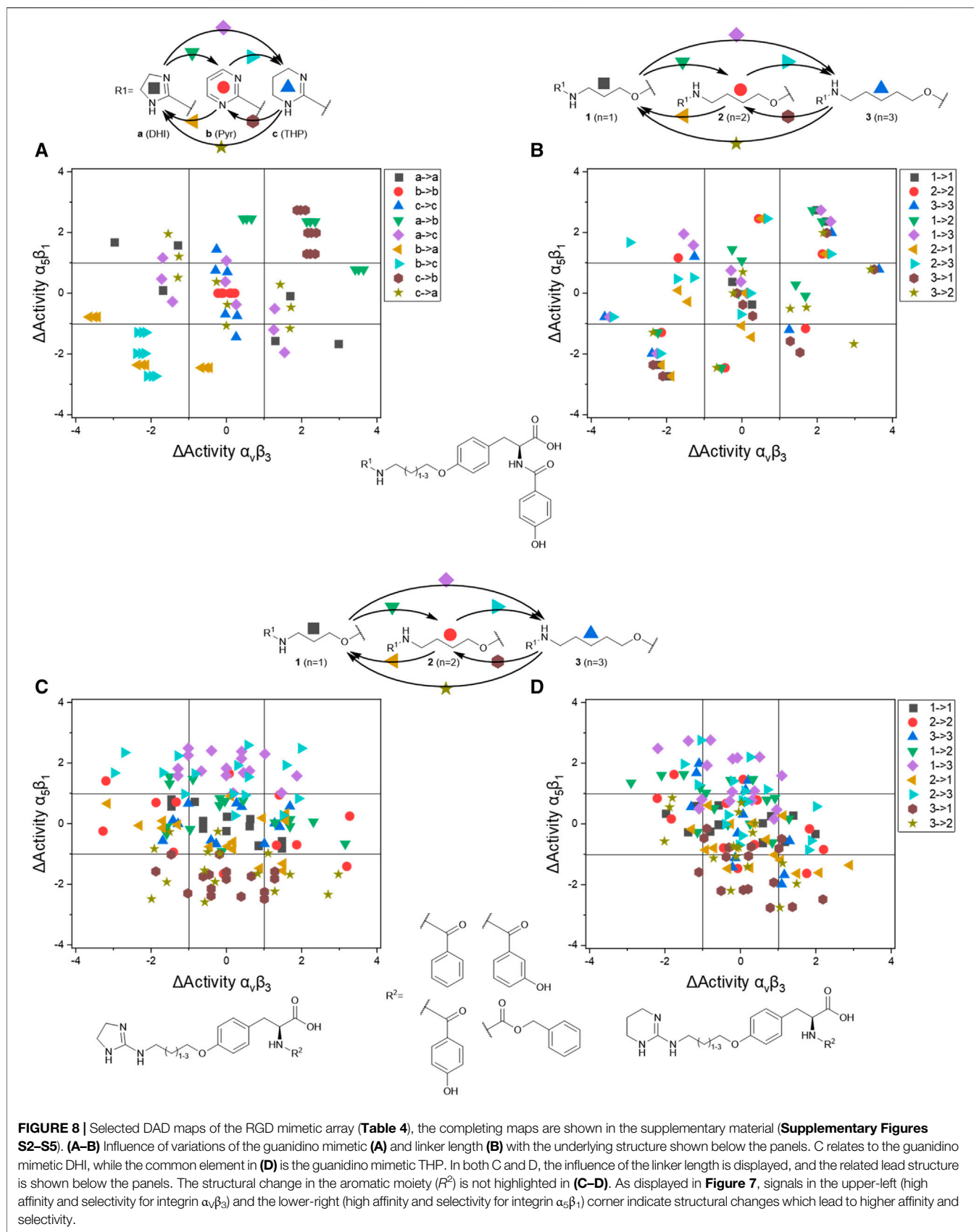


FIGURE 7 | Dual activity and difference map according to Medina-Franco (2012). The areas were selected to assess and present the effect of the structural change they are visible as data points in the corresponding areas.

Figure 8 also indicates that an increasing selectivity is induced by replacing THP by DHI as guanidine mimetic (A) together with increasing affinity/selectivity by longer connector units (B). However, this elongation effect in case of the 4-hydroxybenzoyl derivatives is also influenced by other parameters because of the broad distribution (Figure 8B). Structural changes in presence of other aromatic residues in comparison to 4-hydroxybenzoyl do not lead to significant improvements in selectivity and affinity by changing connector length or the guanidino group (Supplementary Figures S4,S5). Noteworthy, the distribution of 4-hydroxybenzoyl derivatives upon exchanging the guanidino mimetic from DHI or THP to Pyr is narrower than the distribution upon exchanging the guanidino mimetic in presence of the other aromatic moieties (Supplementary Figure S4). This leads to the hypothesis that the influence of introducing a guanidine analog, with a known effect, can be predicted more accurately in presence of this aromatic moiety. Nevertheless, the influence of the aromatic moiety is limited and effects the broad distribution in panels C and D (Figure 8). A more pronounced influence is shown by variation of the connector length between both pharmacophoric groups with either DHI or THP as guanidino mimetics, independently from the aromatic acyl group (panels C and D, Figure 8). This effect is more independent of other structural changes in presence of DHI (C) as guanidino group than with THP (D) whereupon THP leads to greater activity changes (Figure 8). The direct comparison in length changes between DHI (C) and THP (D) substituted derivatives reveals the selectivity dependency of the THP group by accumulating the changes on the descending diagonal (from left-upper to right-down corner) at which a broad distribution is generated (D, Figure 8). In contrast to this observation the length changes from $n = 1$ or 2 to $n = 3$ in presence of DHI resulting in a general decreased activity for



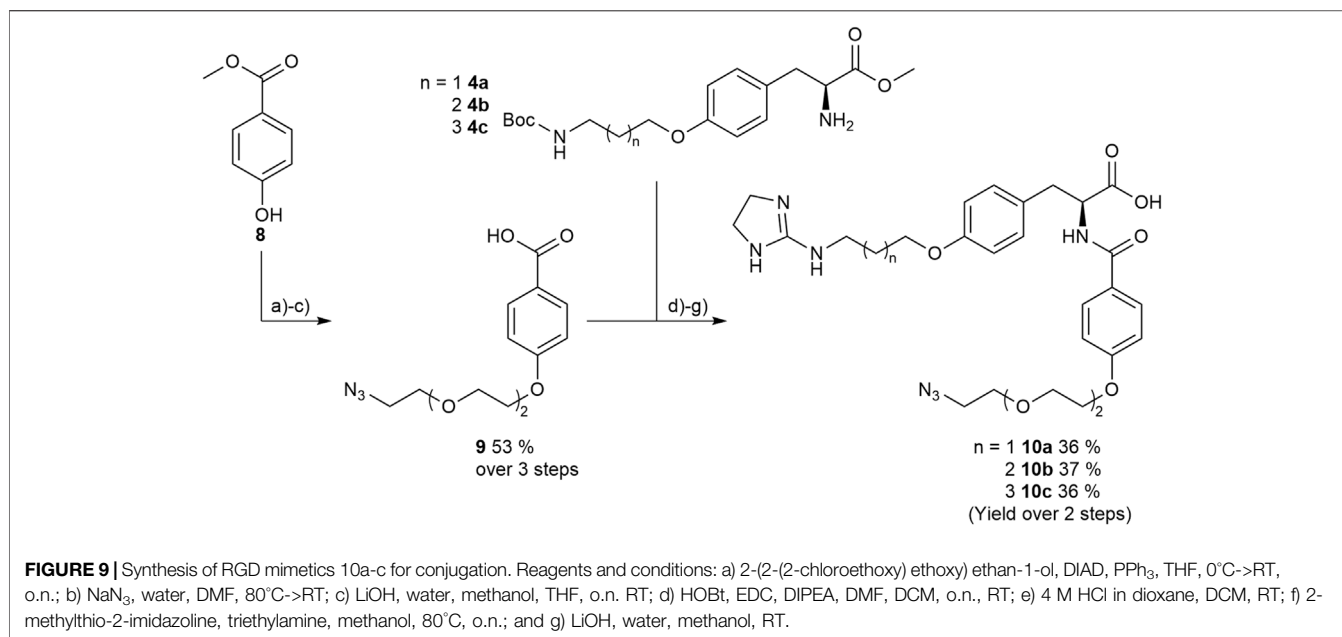


TABLE 5 | Results of the ELISA-like assay for the conjugable RGD mimetics 10a-c (Figure 9).

ID	n =	Integrin $\alpha_V\beta_3$	Integrin $\alpha_5\beta_1$
		IC ₅₀ [nM]	IC ₅₀ [nM]
10a	1	278 ± 69.2	40.0 ± 6.50
10b	2	129 ± 2.35	404 ± 282
10c	3	21.0 ± 5.84	136 ± 27.4
7ba	3	2.01 ± 0.40	1,652 ± 441

integrin $\alpha_5\beta_1$ where at the distribution is more focused (Figure 8C). This leads to the assumption that DHI as guanidino group has a stabilizing effect for predicting biological behavior for structure similar molecules with this moiety.

In summary the DAD mapping analysis of the ELISA results predicts some structural motifs which have great influence on affinity and selectivity for integrin $\alpha_V\beta_3$: A length of $n = 2-3$ whereupon $n = 3$ should be better, 4-hydroxybenzoyl as aromatic moiety and DHI as guanidino group because of its stabilizing effect.

3.4 Synthesis and Biological Evaluation of Conjugable RGD Mimetics

For the implementation of a linear RGD mimetic as homing device for SMDCs it is necessary to incorporate a conjugable function in the RGD mimetic without losing affinity and selectivity for the desired integrin. Based on the DAD mapping analysis DHI as guanidino analog and 4-hydroxybenzoyl was chosen as aromatic moiety because of its biological behavior and simple synthetic modifiability by functionalization with a short azide-containing polyethylene

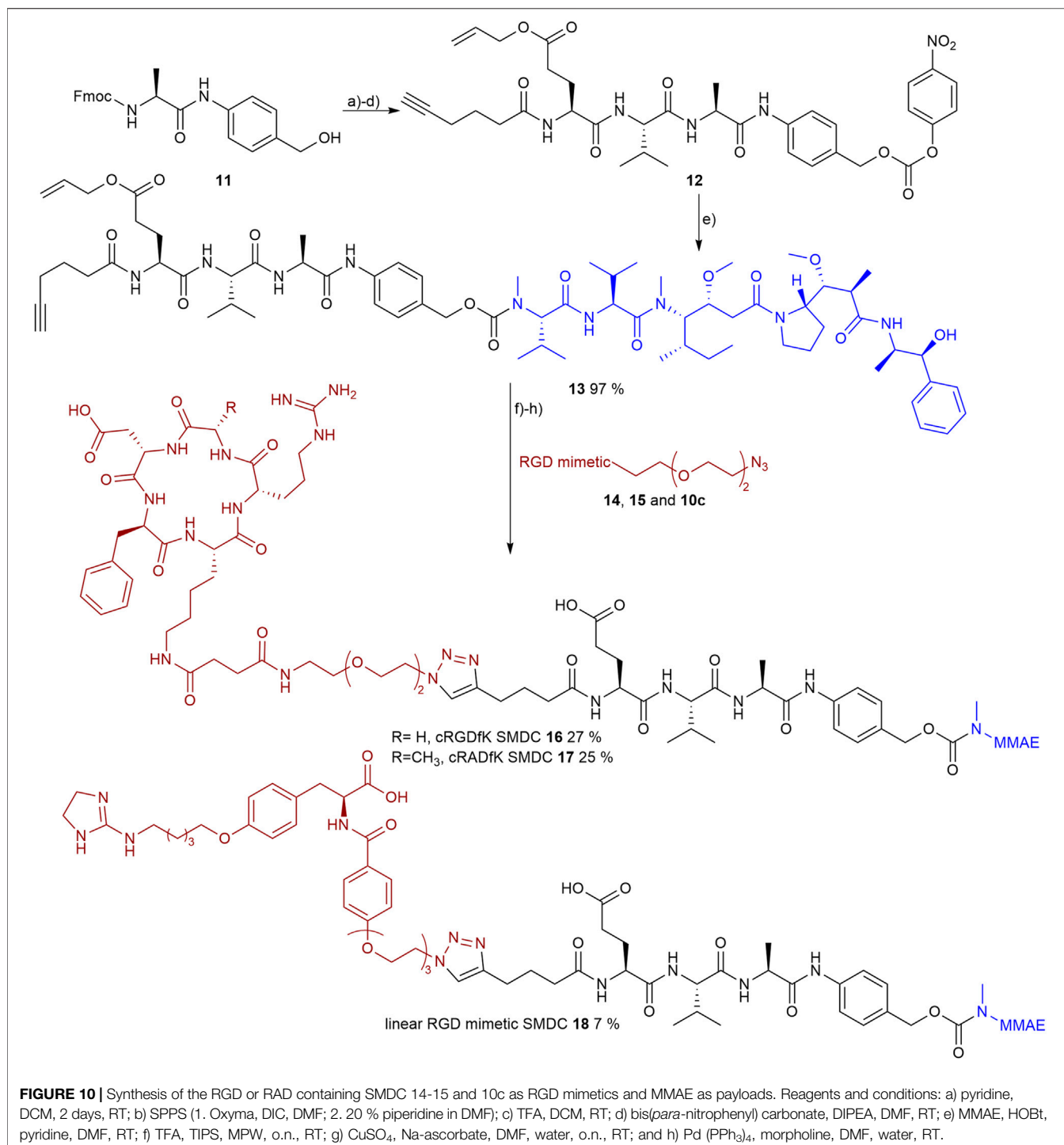
glycol spacer. The conjugation at the para-position of a *N*-terminal aromatic moiety had been investigated for linear mimetics selectively binding integrin $\alpha_V\beta_3$ and $\alpha_5\beta_1$ (Rechenmacher et al., 2013), for piperazine based RGD mimetics (Owen et al., 2007; Klim et al., 2012), and for a tricyclic aminopyrimidine benzoic acid based RGD mimetic (Alsibai et al., 2014). In these cases the decrease in selectivity and activity was only minor.

Therefore, protected 4-hydroxybenzoic acid **8** was modified in a MITSUNOBU reaction with a chlorinated triethylene glycol derivative, followed by azidation using sodium azide. After ester hydrolysis with an excess of LiOH the free acid was coupled with the amines **4a-4c** upon activation with HOBt and EDC to give the three “clickable” RGD mimetics **10a-c** (Figure 9).

The determined IC₅₀ values of compounds **10a-c** (Table 5) validate the predicted influence for the used composition. A higher distance between the carboxylic acid and the guanidino group effects a higher affinity toward integrin $\alpha_V\beta_3$ and a better selectivity over integrin $\alpha_5\beta_1$. However, the triethylene glycol linker attachment in this position decreases the affinity compared to the unconjugated RGD mimetics and negatively influences the selectivity in comparison to **7ba** (Table 5). This negative effect triggered by the linker introduction was also observed for an integrin $\alpha_5\beta_1$ selective linear RGD mimetic where the affinity to integrin $\alpha_V\beta_3$ was increased 13-fold and, consequently, the selectivity was decreased (Rechenmacher et al., 2013).

3.5 Synthesis of cRGDfK and cRADfK Peptides

In order to evaluate the potency of the conjugable RGD mimetic **10c** as a homing device, the peptides cRGDfK and cRADfK were chosen as positive and negative controls due to their difference in



affinity for the $\alpha_v\beta_3$ integrin. The linear peptides were synthesized by solid-phase peptide synthesis using the 2-chlorotrityl resin according to the ^tBu/Fmoc strategy with the coupling reagents oxyma and DIC. Peptide synthesis started with immobilized Fmoc-Gly, as the linear peptide H-Asp (*t*Bu)-D-Phe-Lys (Alloc)-Arg (Pbf)-Gly-OH would not epimerize during macrocyclization with HATU and HOAt. Noteworthy, no epimerization of the C-terminal Ala in H-Asp (*t*Bu)-D-Phe-Lys

(Alloc)-Arg (Pbf)-Ala-OH was observed either. After completion of the *N*-terminal Fmoc protected target peptides on resin, the Alloc group at the lysine side chain was cleaved by Pd catalysis with 1,3-dimethylbarbituric acid (DMBA) as scavenger (Tala et al., 2015). An azide-containing triethylene glycol linker **23** (Supplementary Figure S14) was attached to the lysine side chain on resin using the general coupling protocol GP-6. The linker **23** (Supplementary Figure S9) was synthesized starting

TABLE 6 | Cell adhesion assay of SMDC 16-18 in comparison to Cilengitide. WM115 cells were used as $\alpha_v\beta_3$ -positive cell line and M21-L as $\alpha_v\beta_3$ -negative cell line.

Compound	WM115 ($\alpha_v\beta_3^+$)	M21-L (α_v^- , $\alpha_v\beta_3^-$)
	IC ₅₀ [μ M]	IC ₅₀ [μ M]
Cilengitide	0.43 \pm 0.05	>100 μ M
16	2.65 \pm 0.35	>100 μ M
17	79.1 \pm 1.69	>100 μ M
18	8.05 \pm 0.51	>100 μ M

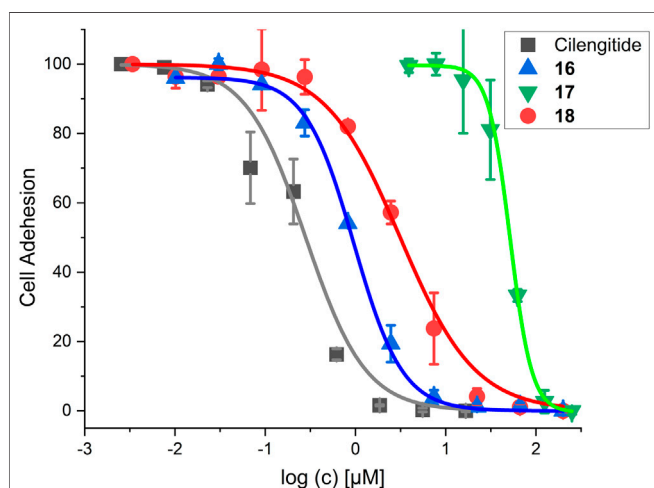


FIGURE 11 | Results for the cell adhesion assay against WM115 cells. For IC₅₀ values, see **Table 6**.

from 2,2'-[ethane-1,2-diylbis(oxy)] bis(ethan-1-ol) following the literature (Gavrilyuk et al., 2009). Afterward the *N*-terminal Fmoc group was cleaved, the peptide was cleaved from the resin using 1% TFA in DCM, and the resulting linear peptides were cyclized under *pseudo*-high dilution (Malesevic et al., 2004) using syringe pumps with separate syringes for the peptide and coupling reagents (see supplementary material). This strategy minimized the number of purification steps to one final normal-phase column chromatography and is more time efficient than the common liquid-phase linker introduction (Gavrilyuk et al., 2009).

3.6 Small-Molecule Drug Conjugate Synthesis

The SMDCs were designed to contain an RGD mimetic as the homing device connected to the antimetabolic drug MMAE as the toxic payload across a self-immolative linker. The dipeptide sequence Val-Ala, cleavable by cathepsin B, was combined with the self-immolative spacer *para*-aminobenzyl carbamate (PABC) to give a lysosomally cleavable conjugate as shown previously in other cases (Dal Corso et al., 2016; Borbély et al., 2019a).

TABLE 7 | Cytotoxicity data with WM115 cells and the calculated targeting index [TI = [IC₅₀ (17)]/[IC₅₀ (compound)]].

Compound	IC ₅₀ [nM]	TI (RAD/RGD)
MMAE	1.84 \pm 0.26	
16 (cRGDfK)	91.4 \pm 12.3	2.9
17 (cRADfK)	264 \pm 24.6	1.0
18 (RGD mimetic)	95.0 \pm 25.0	2.8

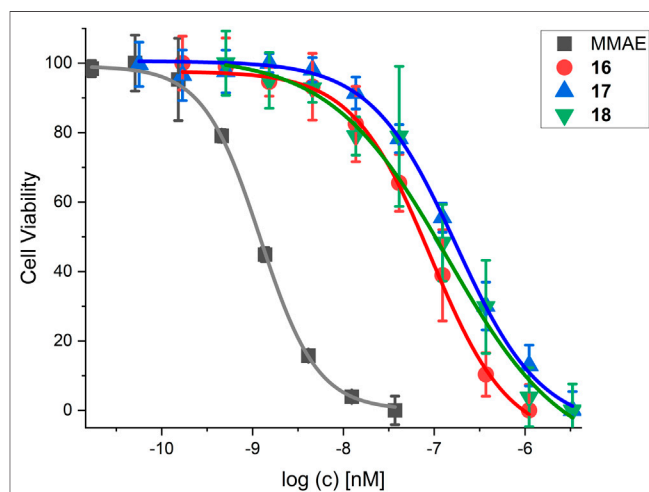


FIGURE 12 | Cell viability assay for SMDC **18** in comparison to control compounds and the free drug MMAE. For IC₅₀ values, see **Table 7**.

An additional glutamic acid was incorporated in the linker to increase the plasma stability (Anami et al., 2018; Poreba, 2020) and 5-hexynoic acid was attached to the *N*-terminal for later conjugation *via* copper-catalyzed azide-alkyne cycloaddition (CuAAC). The linker **12** was synthesized on 2-chlorotrityl resin using the All/Fmoc-strategy and oxyma/DIC as coupling reagents.

The resin was loaded with Fmoc-Val-PABA, obtained from Fmoc-Val and PABA (*para*-aminobenzyl alcohol) using EEDQ-mediated coupling according to the literature (Cheng et al., 2020). The loading was done according to the literature (Barthel et al., 2012) with pyridine as base and gave a loading level of 0.90 mmol/g_{resin}. After coupling of the subsequent amino acids and *N*-terminal 5-hexynoic acid, the peptide was cleaved from the resin and precipitated in water. The resulting benzyl alcohol-containing linker was then activated with bis(*para*-nitrophenyl) carbonate and the resulting (*para*-nitrophenyl) carbonate **12** was coupled to MMAE. As a result of the methylation the *N*-terminal secondary amine of MMAE is sterically hindered and, therefore, the (*para*-nitrophenyl) carbonate **12** has to be activated by the addition of a catalytic amount of HOBt (0.1 eq.) to reach a yield of 97 % after purification *via* normal-phase column chromatography.

Prior to the final CuAAC the side chain-protecting groups of the reference peptides cRGDfK **14** and cRADfK **15** were cleaved using 95% TFA with scavengers. The azide-containing cyclic peptides **14**, **15** or the RGD mimetic **10c** were attached to the alkyne-modified MMAE-linker construct **13** by CuAAC (Figure 10).

3.7 Whole-Cell Evaluation of SMDCs

The RGD mimetic containing SMDC **18** inhibits integrin-dependent cell adhesion, which was shown for WM115 cells presenting the integrin $\alpha_V\beta_3$. The highly affine $\alpha_V\beta_3$ -selective RGD-cyclopeptide Cilengitide was used as reference (Mas-Moruno et al., 2010). The cRGDfK-containing SMDC **16** served as positive control and the cRADfK-containing SMDC **17** as negative control.

The linear RGD SMDC and the cRGDfK SMDC inhibited adhesion of the $\alpha_V\beta_3$ -positive WM115 cells to vitronectin with IC_{50} values in the low μM range, while no effect was observed for the $\alpha_V\beta_3$ -negative M21-L cell line (Table 6 and Figure 11).

The integrin status of the WM115 cells as well as for the control cell line M21-L was determined by fluorescence-activated cell sorting (FACS) analysis. This proved the occurrence of integrins $\alpha_V\beta_3$, $\alpha_V\beta_8$, and $\alpha_5\beta_1$ on WM115 and the absence on M21-L cells except integrin $\alpha_5\beta_1$, which is present (Borbély et al., 2019a) (Supplementary Figure S6).

The cRGDfK-SMDC **16** inhibits cell adhesion of the integrin $\alpha_V\beta_3$ -positive WM115 cells to vitronectin nearly as efficiently as Cilengitide, while the cRADfK-SMDC **17** has a significantly lower effect (Figure 11). Noteworthy, the non-peptide RGD mimetic-SMDC **18** has an IC_{50} value comparable to cRGDfK-SMDC **16**. This is in good agreement with ELISA-like assay results for Cilengitide and the unconjugated linear RGD mimetic **10c** (ELISA IC_{50} : Cilengitide 0.54 nM, **10c** 21.0 nM, Table 5). This corroborates that the RGD mimetic containing SMDC **18** binds to integrin $\alpha_V\beta_3$ like the positive control cRGDfK-SMDC **16**.

The cytotoxicity of SMDC **16-18** was determined in a resazurin based assay with the melanoma cell line WM115 (Table 7 and Figure 12).

MMAE, a cytotoxic agent with a low nM IC_{50} and used as payload in known ADCs and SMDCs (Bai et al., 1990; Staudacher and Brown, 2017; Akaiwa et al., 2020; Criscitiello et al., 2021; Gao et al., 2021), was used as reference compound in the cell viability assay and as SMDC payload. Both the linear RGD SMDC **18** ($IC_{50} = 95.0 \pm 25.0$ nM) and the cRGDfK SMDC **16** ($IC_{50} = 91.4 \pm 12.3$ nM) are about 50-fold less cytotoxic than free MMAE against the $\alpha_V\beta_3$ -positive WM115 cell line with IC_{50} values in the mid-nM range. In contrast, the cRADfK SMDC **17** is 150-fold less cytotoxic than MMAE. Hence, integrin binding also influences the antiproliferative activity. The ratio IC_{50} (RAD)/ IC_{50} (RGD) provides a measure for the selectivity giving a targeting index TI of 2.9 for **16** and 2.8 for **18**. TI values between 1 and 10 have been reported for SMDC (Zanella et al., 2017). Low TI values may also be associated with non-receptor-mediated uptake mechanisms. The size-dependent cellular uptake (Kemker et al., 2019) could be an explanation for this behavior because of the relatively low molecular mass of the conjugates **16-18**. It was also previously reported that a

integrin $\alpha_V\beta_3$ -addressing cRGDfK-carboxyfluorescein conjugate was taken up by integrin-positive and integrin-negative cell lines with the assumption of a fluid-phase uptake (Borbély et al., 2019a).

4 CONCLUSION

Starting from an established tyrosine scaffold, an array of 36 small-molecule RGD mimetics was synthesized by varying three parameters (guanidino mimic, linker length, and aromatic acyl moiety). An efficient diversification strategy was used, which also allows further modifications. The affinities of the RGD mimetics toward the integrins $\alpha_V\beta_3$ and $\alpha_5\beta_1$ were determined in an ELISA-like assay. The DAD mapping analysis of the IC_{50} values allowed to identify important structural motifs to select a conjugable RGD mimetic (**10c**), consisting of DHI (dihydroimidazole) as guanidino mimetic, a C_5 connector, and a 4-hydroxybenzoyl-based azide-containing linker for conjugation. The mimetic **10c** was connected by CuAAC to a cathepsin-cleavable linker **13**, where the Val-Ala recognition sequence was linked across a self-immolative PABC (*para*-aminobenzyl carbamate) moiety to MMAE, giving the RGD mimetic-SMDC **18**. Peptide conjugates like the cRGDfK-SMDC **16** as the positive control and the cRADfK-SMDC **17** as the negative control were investigated with respect to integrin binding in cell adhesion assays. The positive control cRGDfK-SMDC **16** and the RGD mimetic-SMDC **18** displayed micromolar IC_{50} values with $\alpha_V\beta_3$ -positive cells, while no influence on cell adhesion was observed for $\alpha_V\beta_3$ -negative cells, which indicates a receptor selectivity for SMDC **16** and **18**. The cell viability assay revealed cytotoxicity in the nanomolar range for SMDC **16** and **18**. Hence, integrin binding also influences the antiproliferative activity giving a targeting index of 2.8. Thus, a bioactive SMDC was obtained based on a linear RGD mimetic retrieved by DAD mapping analysis of a small-molecule array and the resulting structural prediction.

DATA AVAILABILITY STATEMENT

The original contributions presented in the study are included in the article/Supplementary Material, further inquiries can be directed to the corresponding author.

AUTHOR CONTRIBUTIONS

Conceptualization: JP; investigation: JP; resources: NS; supervision: NS; validation: JP; and writing—original draft: JP; writing—review and editing: NS. All authors have read and agreed upon the final version of the manuscript.

ACKNOWLEDGMENTS

The authors thank Beate Nachtigall and Lennard Karsten for their support in the flow cytometry experiments and Carmela

Michalek for performing the cell adhesion and cell viability assays. We acknowledge the financial support from the German Research Foundation (DFG) and the Open Access Publication Fund of Bielefeld University for the article processing charge.

REFERENCES

- Akaiwa, M., Dugal-Tessier, J., and Mendelsohn, B. A. (2020). Antibody-Drug Conjugate Payloads; Study of Auristatin Derivatives. *Chem. Pharm. Bull.* 68, 201–211. doi:10.1248/cpb.c19-00853
- Alsibai, W., Hahnenkamp, A., Eisenblätter, M., Riemann, B., Schäfers, M., Bremer, C., et al. (2014). Fluorescent Non-peptidic RGD Mimetics with High Selectivity for $\alpha_v\beta_3$ vs $\alpha_{IIb}\beta_3$ Integrin Receptor: Novel Probes for *In Vivo* Optical Imaging. *J. Med. Chem.* 57, 9971–9982. doi:10.1021/jm501197c
- Anami, Y., Yamazaki, C. M., Xiong, W., Gui, X., Zhang, N., An, Z., et al. (2018). Glutamic Acid-Valine-Citrulline Linkers Ensure Stability And Efficacy Of Antibody-Drug Conjugates In Mice. *Nat. Commun.* 9, 2512. doi:10.1038/s41467-018-04982-3
- Anselmi, M., Borbély, A., Figueras, E., Michalek, C., Kemker, I., Gentilucci, L., et al. (2020). Linker Hydrophilicity Modulates the Anticancer Activity of RGD-Cryptophycin Conjugates. *Chem. Eur. J.* 27, 1015–1022. doi:10.1002/chem.202003471
- Aumailley, M., Gurrath, M., Müller, G., Calvete, J., Timpl, R., and Kessler, H. (1991). Arg-Gly-Asp Constrained within Cyclic Pentapeptides Strong and Selective Inhibitors of Cell Adhesion to Vitronectin and Laminin Fragment P1. *FEBS Lett.* 291, 50–54. doi:10.1016/0014-5793(91)81101-D
- Bachmann, M., Kukkurainen, S., Hytönen, V. P., and Wehrle-Haller, B. (2019). Cell Adhesion by Integrins. *Physiol. Rev.* 99, 1655–1699. doi:10.1152/physrev.00036.2018
- Bai, R., Petit, G. R., and Hamel, E. (1990). Dolastatin 10, a Powerful Cytostatic Peptide Derived from a marine Animal. *Biochem. Pharmacol.* 39, 1941–1949. doi:10.1016/0006-2952(90)90613-P
- Baiula, M., Cirillo, M., Martelli, G., Giraldi, V., Gasparini, E., Anelli, A. C., et al. (2021). Selective Integrin Ligands Promote Cell Internalization of the Antineoplastic Agent Fluorouracil. *ACS Pharmacol. Transl. Sci.* 4, 1528–1542. doi:10.1021/acspsci.1c00094
- Barczyk, M., Carracedo, S., and Gullberg, D. (2010). Integrins. *Cell Tissue Res* 339, 269–280. doi:10.1007/s00441-009-0834-6
- Bargh, J. D., Isidro-Llobet, A., Parker, J. S., and Spring, D. R. (2019). Cleavable Linkers in Antibody-Drug Conjugates. *Chem. Soc. Rev.* 48, 4361–4374. doi:10.1039/C8CS00676H
- Barthel, B. L., Rudnicki, D. L., Kirby, T. P., Colvin, S. M., Burkhart, D. J., and Koch, T. H. (2012). Synthesis and Biological Characterization of Protease-Activated Prodrugs of Doxazolidine. *J. Med. Chem.* 55, 6595–6607. doi:10.1021/jm300714p
- Battistini, L., Bugatti, K., Sartori, A., Curti, C., and Zanardi, F. (2021). RGD Peptide-Drug Conjugates as Effective Dual Targeting Platforms: Recent Advances. *Eur. J. Org. Chem.* 2021, 2506–2528. doi:10.1002/ejoc.202100240
- Bochen, A., Marelli, U. K., Otto, E., Pallarola, D., Mas-Moruno, C., Di Leva, F. S., et al. (2013). Biselectivity of isoDGR Peptides for Fibronectin Binding Integrin Subtypes $\alpha_5\beta_1$ and $\alpha_v\beta_6$: Conformational Control through Flanking Amino Acids. *J. Med. Chem.* 56, 1509–1519. doi:10.1021/jm301221x
- Borbély, A., Figueras, E., Martins, A., Boder, L., Raposo Moreira Dias, A., López Rivas, P., et al. (2019a). Conjugates of Cryptophycin and RGD or Iso DGR Peptidomimetics for Targeted Drug Delivery. *ChemistryOpen* 8, 737–742. doi:10.1002/open.201900110
- Borbély, A., Figueras, E., Martins, A., Esposito, S., Auciello, G., Monteagudo, E., et al. (2019b). Synthesis and Biological Evaluation of RGD-Cryptophycin Conjugates for Targeted Drug Delivery. *Pharmaceutics* 11, 151. doi:10.3390/pharmaceutics11040151
- Casi, G., and Neri, D. (2015). Antibody-Drug Conjugates and Small Molecule-Drug Conjugates: Opportunities and Challenges for the Development of Selective Anticancer Cytotoxic Agents. *J. Med. Chem.* 58, 8751–8761. doi:10.1021/acs.jmedchem.5b00457
- Chari, R. V. J., Miller, M. L., and Widdison, W. C. (2014). Antibody-drug Conjugates: an Emerging Concept in Cancer Therapy. *Angew. Chem. Int. Ed.* 53, 3796–3827. doi:10.1002/anie.201307628
- Cheng, P., Miao, Q., Huang, J., Li, J., and Pu, K. (2020). Multiplex Optical Urinalysis for Early Detection of Drug-Induced Kidney Injury. *Anal. Chem.* 92, 6166–6172. doi:10.1021/acs.analchem.0c00989
- Cooper, J., and Giancotti, F. G. (2019). Integrin Signaling in Cancer: Mechanotransduction, Stemness, Epithelial Plasticity, and Therapeutic Resistance. *Cancer Cell* 35, 347–367. doi:10.1016/j.ccell.2019.01.007
- Corbett, J. W., Graciani, N. R., Mousa, S. A., and DeGrado, W. F. (1997). Solid-phase Synthesis of a Selective $\alpha_v\beta_3$ Integrin Antagonist Library. *Bioorg. Med. Chem. Lett.* 7, 1371–1376. doi:10.1016/S0960-894X(97)00200-X
- Criscitello, C., Morganti, S., and Curigliano, G. (2021). Antibody-drug Conjugates in Solid Tumors: a Look into Novel Targets. *J. Hematol. Oncol.* 14, 20. doi:10.1186/s13045-021-01035-z
- Curley, G. P., Blum, H., and Humphries, M. J. (1999). Integrin Antagonists. *Cell Mol. Life Sci.* 56, 427–441. doi:10.1007/s000180050443
- Dal Corso, A., Pignataro, L., Belvisi, L., and Gennari, C. (2016). $\alpha_v\beta_3$ Integrin-Targeted Peptide/Peptidomimetic-Drug Conjugates: In-Depth Analysis of the Linker Technology. *Curr. Top. Med. Chem.* 16, 314–329. doi:10.2174/1568026615666150701114343
- De Franceschi, N., Hamidi, H., Alanko, J., Sahgal, P., and Ivaska, J. (2015). Integrin Traffic - the Update. *J. Cell Sci.* 128, 839–852. doi:10.1242/jcs.161653
- Deneka, A. Y., Bumber, Y., Beck, T., and Golemis, E. A. (2019). Tumor-Targeted Drug Conjugates as an Emerging Novel Therapeutic Approach in Small Cell Lung Cancer (SCLC). *Cancers* 11, 1297. doi:10.3390/cancers11091297
- Deonarain, M., Yahioğlu, G., Stamati, I., Pomowski, A., Clarke, J., Edwards, B., et al. (2018). Small-Format Drug Conjugates: A Viable Alternative to ADCs for Solid Tumours? *Antibodies* 7, 16. doi:10.3390/antib7020016
- Egbertson, M. S., Chang, C. T., Duggan, M. E., Gould, R. J., Halczenko, W., Hartman, G. D., et al. (1994). Non-Peptide Fibrinogen Receptor Antagonists. 2. Optimization of a Tyrosine Template as a Mimic For Arg-Gly-Asp. *J. Med. Chem.* 37, 2537–2551. doi:10.1021/jm00042a007
- Eliceiri, B. P., and Cheresh, D. A. (1999). The Role of α_v Integrins during Angiogenesis: Insights into Potential Mechanisms of Action and Clinical Development. *J. Clin. Invest.* 103, 1227–1230. doi:10.1172/JCI6869
- Engel, J., Emons, G., Pinski, J., and Schally, A. V. (2012). AEZS-108: a Targeted Cytotoxic Analog of LHRH for the Treatment of Cancers Positive for LHRH Receptors. *Expert Opin. Investig. Drugs* 21, 891–899. doi:10.1517/13543784.2012.685128
- Frank, A. O., Otto, E., Mas-Moruno, C., Schiller, H. B., Marinelli, L., Cosconati, S., et al. (2010). Conformational Control of Integrin-Subtype Selectivity in isoDGR Peptide Motifs: a Biological Switch. *Angew. Chem. Int. Edition* 49, 9278–9281. doi:10.1002/anie.201004363
- Gao, G., Wang, Y., Hua, H., Li, D., and Tang, C. (2021). Marine Antitumor Peptide Dolastatin 10: Biological Activity, Structural Modification and Synthetic Chemistry. *Mar. Drugs* 19, 363. doi:10.3390/md19070363
- Gavrilyuk, J. I., Wuellner, U., and Barbas, C. F. (2009). β -Lactam-based Approach for the Chemical Programming of Aldolase Antibody 38C2. *Bioorg. Med. Chem. Lett.* 19, 1421–1424. doi:10.1016/j.bmcl.2009.01.028
- Gerber, H.-P., Senter, P. D., and Grewal, I. S. (2009). Antibody Drug-Conjugates Targeting the Tumor Vasculature. *MABS* 1, 247–253. doi:10.4161/mabs.1.3.8515
- Giancotti, F. G., and Ruoslahti, E. (1999). Integrin Signaling. *Science* 285, 1028–1033. doi:10.1126/science.285.5430.1028
- Gurrath, M., Müller, G., Kessler, H., Aumailley, M., and Timpl, R. (1992). Conformation/activity Studies of Rationally Designed Potent Anti-adhesive

SUPPLEMENTARY MATERIAL

The Supplementary Material for this article can be found online at: <https://www.frontiersin.org/articles/10.3389/fchem.2022.869639/full#supplementary-material>

- RGD Peptides. *Eur. J. Biochem.* 210, 911–921. doi:10.1111/j.1432-1033.1992.tb17495.x
- Haubner, R., Finsinger, D., and Kessler, H. (1997). Stereoisomeric Peptide Libraries and Peptidomimetics for Designing Selective Inhibitors of The $\alpha_v\beta_3$ Integrin for a New Cancer Therapy. *Angew. Chem. Int. Ed. Engl.* 36, 1374–1389. doi:10.1002/anie.199713741
- Heckmann, D., Laufer, B., Marinelli, L., Limongelli, V., Novellino, E., Zahn, G., et al. (2009). Breaking the Dogma of the Metal-Coordinating Carboxylate Group in Integrin Ligands: Introducing Hydroxamic Acids to the MIDAS to Tune Potency and Selectivity. *Angew. Chem. Int. Ed.* 48, 4436–4440. doi:10.1002/anie.200900206
- Heckmann, D., Meyer, A., Laufer, B., Zahn, G., Stragies, R., and Kessler, H. (2008). Rational Design of Highly Active and Selective Ligands for the $\alpha_5\beta_1$ Integrin Receptor. *Chembiochem* 9, 1397–1407. doi:10.1002/cbic.200800045
- Heckmann, D., Meyer, A., Marinelli, L., Zahn, G., Stragies, R., and Kessler, H. (2007). Probing Integrin Selectivity: Rational Design of Highly Active and Selective Ligands for the $\alpha_5\beta_1$ and $\alpha_v\beta_3$ Integrin Receptor. *Angew. Chem. Int. Ed.* 46, 3571–3574. doi:10.1002/anie.200700008
- Hoppenz, P., Els-Heindl, S., Beck-Sickinger, A. G., Els-Heindl, S., and Beck-Sickinger, A. G. (2020). Peptide-Drug Conjugates and Their Targets in Advanced Cancer Therapies. *Front. Chem.* 8, 571. doi:10.3389/fchem.2020.00571
- Humphries, J. D., Byron, A., and Humphries, M. J. (2006). Integrin Ligands at a Glance. *J. Cell Sci* 119, 3901–3903. doi:10.1242/jcs.03098
- Hynes, R. O. (2002). Integrins. *Cell* 110, 673–687. doi:10.1016/S0092-8674(02)00971-6
- Jin, Z.-H., Furukawa, T., Ohya, T., Degardin, M., Sugyo, A., Tsuji, A. B., et al. (2017). ^{67}Cu -Radiolabeling of a Multimeric RGD Peptide for $\alpha_v\beta_3$ Integrin-Targeted Radionuclide Therapy. *Nucl. Med. Commun.* 38, 347–355. doi:10.1097/MNM.0000000000000646
- Kapp, T. G., Fottner, M., Maltsev, O. V., and Kessler, H. (2016). Small Cause, Great Impact: Modification of the Guanidine Group in the RGD Motif Controls Integrin Subtype Selectivity. *Angew. Chem. Int. Ed.* 55, 1540–1543. doi:10.1002/anie.201508713
- Kapp, T. G., Rechenmacher, F., Neubauer, S., Maltsev, O. V., Cavalcanti-Adam, E. A., Zarka, R., et al. (2017). A Comprehensive Evaluation of the Activity and Selectivity Profile of Ligands for RGD-Binding Integrins. *Sci. Rep.* 7, 39805. doi:10.1038/srep39805
- Kemker, I., Feiner, R. C., Müller, K. M., and Sewald, N. (2019). Size-Dependent Cellular Uptake Of RGD Peptides. *Chembiochem*. doi:10.1002/cbic.201900512
- Kemker, I., Schröder, D. C., Feiner, R. C., Müller, K. M., Marion, A., and Sewald, N. (2021). Tuning the Biological Activity of RGD Peptides with Halotryptophans. *J. Med. Chem.* 64, 586–601. doi:10.1021/acs.jmedchem.0c01536
- Khongorzul, P., Ling, C. J., Khan, F. U., Ihsan, A. U., and Zhang, J. (2020). Antibody-Drug Conjugates: A Comprehensive Review. *Mol. Cancer Res.* 18, 3–19. doi:10.1158/1541-7786.MCR-19-0582
- Klim, J. R., Fowler, A. J., Courtney, A. H., Wrighton, P. J., Sheridan, R. T. C., Wong, M. L., et al. (2012). Small-Molecule-Modified Surfaces Engage Cells through the $\alpha_v\beta_3$ Integrin. *ACS Chem. Biol.* 7, 518–525. doi:10.1021/cb2004725
- Lerchen, H.-G., Stelte-Ludwig, B., Kopitz, C., Heroult, M., Zubov, D., Willuda, J., et al. (2022). A Small Molecule-Drug Conjugate (SMDC) Consisting of a Modified Camptothecin Payload Linked to an $\alpha_v\beta_3$ Binder for the Treatment of Multiple Cancer Types. *Cancers* 14, 391. doi:10.3390/cancers14020391
- Malesevic, M., Strijowski, U., Bächle, D., and Sewald, N. (2004). An Improved Method for the Solution Cyclization of Peptides under Pseudo-high Dilution Conditions. *J. Biotechnol.* 112, 73–77. doi:10.1016/j.jbiotec.2004.03.015
- Marinelli, L., Meyer, A., Heckmann, D., Lavecchia, A., Novellino, E., and Kessler, H. (2005). Ligand Binding Analysis For Human $\alpha_5\beta_1$ Integrin: Strategies For Designing New $\alpha_5\beta_1$ Integrin Antagonists. *J. Med. Chem.* 48, 4204–4207. doi:10.1021/jm040224i
- Mas-Moruno, C., Rechenmacher, F., and Kessler, H. (2010). Cilengitide: The First Anti-Angiogenic Small Molecule Drug Candidate Design, Synthesis And Clinical Evaluation. *Anti-Cancer Agents Med. Chem.* 10, 753–768. doi:10.2174/187152010794728639
- Mas-Moruno, C., Fraioli, R., Rechenmacher, F., Neubauer, S., Kapp, T. G., and Kessler, H. (2016a). $\alpha_v\beta_3$ - oder $\alpha_5\beta_1$ -Integrin-selektive Peptidmimetika für die Oberflächenbeschichtung. *Angew. Chem.* 128, 7162–7183. doi:10.1002/ange.201509782
- Mas-Moruno, C., Fraioli, R., Rechenmacher, F., Neubauer, S., Kapp, T. G., and Kessler, H. (2016b). $\alpha_v\beta_3$ - or $\alpha_5\beta_1$ -Integrin-Selective Peptidomimetics for Surface Coating. *Angew. Chem. Int. Ed.* 55, 7048–7067. doi:10.1002/anie.201509782
- Medina-Franco, J. L., Edwards, B. S., Pinilla, C., Appel, J. R., Giulianotti, M. A., Santos, R. G., et al. (2013). Rapid Scanning Structure-Activity Relationships in Combinatorial Data Sets: Identification of Activity Switches. *J. Chem. Inf. Model.* 53, 1475–1485. doi:10.1021/ci400192y
- Medina-Franco, J. L. (2012). Scanning Structure-Activity Relationships with Structure-Activity Similarity and Related Maps: from Consensus Activity Cliffs to Selectivity Switches. *J. Chem. Inf. Model.* 52, 2485–2493. doi:10.1021/ci300362x
- Medina-Franco, J. L., Yongye, A. B., Pérez-Villanueva, J., Houghten, R. A., and Martínez-Mayorga, K. (2011). Multitarget Structure-Activity Relationships Characterized by Activity-Difference Maps and Consensus Similarity Measure. *J. Chem. Inf. Model.* 51, 2427–2439. doi:10.1021/ci200281v
- Nagy, A., Schally, A. V., Armatis, P., Szepeshazi, K., Halmos, G., Kovacs, M., et al. (1996). Cytotoxic Analogs of Luteinizing Hormone-Releasing Hormone Containing Doxorubicin or 2-pyrrolinodoxorubicin, a Derivative 500-1000 Times More Potent. *Proc. Natl. Acad. Sci.* 93, 7269–7273. doi:10.1073/pnas.93.14.7269
- Nahrwold, M., Weiß, C., Bogner, T., Mertink, F., Conradi, J., Sammet, B., et al. (2013). Conjugates of Modified Cryptophycins and RGD-Peptides Enter Target Cells by Endocytosis. *J. Med. Chem.* 56, 1853–1864. doi:10.1021/jm301346z
- Nieberler, M., Reuning, U., Reichart, F., Notni, J., Wester, H.-J., Schwaiger, M., et al. (2017). Exploring the Role of RGD-Recognizing Integrins in Cancer. *Cancers* 9, 116. doi:10.3390/cancers9090116
- Owen, R. M., Carlson, C. B., Xu, J., Mowery, P., Fasella, E., and Kiessling, L. L. (2007). Bifunctional Ligands that Target Cells Displaying the $\alpha_v\beta_3$ Integrin. *Chembiochem* 8, 68–82. doi:10.1002/cbic.200600339
- Pérez-Villanueva, J., Santos, R., Hernández-Campos, A., Giulianotti, M. A., Castillo, R., and Medina-Franco, J. L. (2011). Structure-activity Relationships of Benzimidazole Derivatives as Antiparasitic Agents: Dual Activity-Difference (DAD) Maps. *Med. Chem. Commun.* 2, 44–49. doi:10.1039/c0md00159g
- Pina, A., Dal Corso, A., Caruso, M., Belvisi, L., Arosio, D., Zanella, S., et al. (2017). Targeting Integrin $\alpha_v\beta_3$ with Theranostic RGD-Camptothecin Conjugates Bearing a Disulfide Linker: Biological Evaluation Reveals a Complex Scenario. *ChemistrySelect* 2, 4759–4766. doi:10.1002/slct.201701052
- Poreba, M. (2020). Protease-Activated Prodrugs: Strategies, Challenges, And Future Directions. *FEBS J.* 287, 1936–1969. doi:10.1111/febs.15227
- Rechenmacher, F., Neubauer, S., Polleux, J., Mas-Moruno, C., De Simone, M., Cavalcanti-Adam, E. A., et al. (2013). Functionalizing $\alpha_v\beta_3$ - or $\alpha_5\beta_1$ -Selective Integrin Antagonists for Surface Coating: A Method to Discriminate Integrin Subtypes *In Vitro*. *Angew. Chem. Int. Ed.* 52, 1572–1575. doi:10.1002/anie.201206370
- Rékási, Z., Szöke, B., Nagy, A., Groot, K., Rékási, E. S., and Schally, A. V. (1993). Effect of Luteinizing Hormone-Releasing Hormone Analogs Containing Cytotoxic Radicals on the Function of Rat Pituitary Cells: Tests in a Long Term Superfusion System. *Endocrinology* 132, 1991–2000. doi:10.1210/endo.132.5.8477650
- Rockwell, A. L., Rafalski, M., Pitts, W. J., Batt, D. G., Petraitis, J. J., DeGrado, W. F., et al. (1999). Rapid Synthesis of RGD Mimetics with Isoxazoline Scaffolds on Solid Phase: Identification of $\alpha_v\beta_3$ Antagonists lead Compounds. *Bioorg. Med. Chem. Lett.* 9, 937–942. doi:10.1016/S0960-894X(99)00114-6
- Schaffner, F., Ray, A., and Dontenwill, M. (2013). Integrin $\alpha_5\beta_1$, the Fibronectin Receptor, as a Pertinent Therapeutic Target in Solid Tumors. *Cancers* 5, 27–47. doi:10.3390/cancers5010027
- Slack, R. J., Macdonald, S. J. F., Roper, J. A., Jenkins, R. G., and Hatley, R. J. D. (2022). Emerging Therapeutic Opportunities for Integrin Inhibitors. *Nat. Rev. Drug Discov.* 21, 60–78. doi:10.1038/s41573-021-00284-4
- Srinivasarao, M., Galliford, C. V., and Low, P. S. (2015). Principles in the Design of Ligand-Targeted Cancer Therapeutics and Imaging Agents. *Nat. Rev. Drug Discov.* 14, 203–219. doi:10.1038/nrd4519
- Staudacher, A. H., and Brown, M. P. (2017). Antibody Drug Conjugates and Bystander Killing: Is Antigen-dependent Internalisation Required? *Br. J. Cancer* 117, 1736–1742. doi:10.1038/bjc.2017.367
- Tala, S. R., Schnell, S. M., and Haskell-Luevano, C. (2015). Microwave-Assisted Solid-Phase Synthesis of Side-Chain to Side-Chain Lactam-Bridge Cyclic Peptides. *Bioorg. Med. Chem. Lett.* 25, 5708–5711. doi:10.1016/j.bmcl.2015.10.095

Wei, B., Gunzner-Toste, J., Yao, H., Wang, T., Wang, J., Xu, Z., et al. (2018). Discovery of Peptidomimetic Antibody-Drug Conjugate Linkers with Enhanced Protease Specificity. *J. Med. Chem.* 61, 989–1000. doi:10.1021/acs.jmedchem.7b01430

Zanella, S., Angerani, S., Pina, A., López Rivas, P., Giannini, C., Panzeri, S., et al. (2017). Tumor Targeting with an Iso DGR-Drug Conjugate. *Chem. Eur. J.* 23, 7910–7914. doi:10.1002/chem.201701844

Conflict of Interest: The authors declare that the research was conducted in the absence of any commercial or financial relationships that could be construed as a potential conflict of interest.

Publisher's Note: All claims expressed in this article are solely those of the authors and do not necessarily represent those of their affiliated organizations, or those of the publisher, the editors, and the reviewers. Any product that may be evaluated in this article, or claim that may be made by its manufacturer, is not guaranteed or endorsed by the publisher.

Copyright © 2022 Paulus and Sewald. This is an open-access article distributed under the terms of the Creative Commons Attribution License (CC BY). The use, distribution or reproduction in other forums is permitted, provided the original author(s) and the copyright owner(s) are credited and that the original publication in this journal is cited, in accordance with accepted academic practice. No use, distribution or reproduction is permitted which does not comply with these terms.